Submitted, accepted and published by:
Chemical Engineering Journal 258 (2014) 265-280

Kinetic determination of a highly reactive impregnated Fe_2O_3/Al_2O_3 oxygen carrier for use in gas-fuelled Chemical Looping Combustion

A. Cabello, A. Abad*, F. García-Labiano, P. Gayán, L. F. de Diego, J. Adánez

Instituto de Carboquímica (ICB-CSIC), Department of Energy and Environment,

Miguel Luesma Castán 4, Zaragoza 50018, SPAIN.

* Corresponding author. Tel.: +34 976 733 977. Fax: +34 976 733 318. E-mail address: abad@icb.csic.es (Alberto Abad)

Abstract

The objective of this work was to determine the kinetic parameters for reduction and oxidation reactions of a highly reactive Fe-based oxygen carrier for use in chemical looping combustion (CLC) of gaseous fuels containing CH_4, CO and/or H_2, e.g. natural gas, syngas and PSA-off gas. The oxygen carrier was prepared by impregnation of iron on alumina. The effect of both the temperature and gas concentration was analysed in a thermogravimetric analyser (TGA).

The grain model with uniform conversion in the particle and reaction in grains following the shrinking core model (SCM) was used for kinetics determination. It was

assumed that the reduction reactions were controlled by two different resistances: the reaction rate was controlled by chemical reaction in a first step, whereas the mechanism that controlled the reactions at higher conversion values was diffusion through the product layer around the grains. Furthermore, it was found that the reduction reaction mechanism was based on the interaction of Fe_2O_3 with Al_2O_3 in presence of the reacting gases to form $FeAl_2O_4$ as the only stable Fe-based phase. The reaction order values found for the reducing gases were 0.25, 0.3 and 0.6 for CH_4, H_2 and CO, respectively, and the activation energy took values of between 8 kJ mol^{-1} (for H_2) and 66 kJ mol^{-1} (for CH_4). With regard to oxidation kinetics, the reacting model assumed a reaction rate that was only controlled by chemical reaction. Values of 0.9 and 23 kJ mol^{-1} were found for reaction order and activation energy, respectively.

Finally, the solids inventory needed in a CLC system was also estimated by considering kinetic parameters. The total solids inventory in the CLC unit took a minimum value of 150 kg MW^{-1} for CH_4 combustion, which is a low value when compared to those of other Fe-based materials found in the literature.

Keywords

CO_2 capture, Chemical looping combustion, Oxygen carrier, Iron, Reaction kinetic, Impregnated.

1. Introduction

The Intergovernmental Panel on Climate Change [1] concluded in 2013 that climate change is unequivocal and that its main cause is human activity. In order to avoid an excessive increase in the average temperature in the Earth, which could lead to

unpredictable consequences, it is necessary to apply mitigation measures to reduce worldwide greenhouse gas emissions. Carbon Capture and Storage (CCS) technologies have been proposed as a transitory measure until other competitive CO_2 emission-free technologies are demonstrated. CCS is a process consisting of the separation of CO_2 from industrial and energy-related sources, transport to a storage location and long-term isolation from the atmosphere [2]. According to the IPCC [2], CCS technologies will play a significant role in reducing CO_2 emissions and stabilizing its concentration in the atmosphere with reasonable cost-effectiveness, mitigating its negative effects on the environment. The main disadvantages of these technologies are their higher initial costs and the energy penalty on the overall combustion process. In this context, over the last years there has been considerable growth in interest in developing new, cost-effective combustion processes that generate highly concentrated CO_2 streams. One of these new processes is Chemical Looping Combustion (CLC) which has emerged as an environmentally-acceptable alternative for energy production from fossil fuels given that CO_2 separation is inherent to the actual combustion process.

The concept on which the CLC process is based was first proposed in 1954 by Lewis and Gilligand [3] to produce pure CO_2 from fossil fuels. Three decades later, in 1983, Ritcher and Knoche [4] presented CLC technology as a suitable process with which to increase the thermal efficiency of a power plant, which was supported by works performed by Ishida et al. [5-7]. At the beginning of the current century Lyngfelt et al. [8] proposed CLC for the capture CO_2 at a low cost. The CLC design was based on two interconnected fluidized beds with a solid, known as an oxygen carrier, circulating between them. This oxygen carrier is often composed of a metal oxide, which is the source of oxygen in this process, and an inert material which acts as support in order to

increase mechanical strength. The main role of this oxygen carrier is to prevent the direct contact between fuel and air during the combustion process, for which this material is circulated between two reactors: the fuel reactor, where the reduction of the oxygen carrier and combustion of the fuel take place, and the air reactor, where the oxygen carrier is oxidized.

One key aspect for optimum performance of a CLC system is the oxygen carrier, which has to be able to fully convert the fuel to CO_2 and H_2O and to present high reactivity with the fuel and air throughout a large number of redox cycles. Furthermore, it must fulfil other characteristics, such as high attrition resistance and not presenting any problems of agglomeration or carbon deposition. Finally, environmental and economic aspects must be also considered for the final selection of an optimum oxygen carrier [9]. Iron-based oxygen carriers are gaining considerable importance for the CLC process, since they present better environmental compatibility and a lower cost in comparison with other metal oxides. These oxygen carriers have shown adequate reactivity under atmospheric [10-12] and pressurized [13] conditions and high reactivity with CO and H_2, and do not present thermodynamic limitations to fully convert CH_4, CO and H_2 to CO_2 and H_2O if the reduction of the iron oxide, in the form of haematite (Fe_2O_3), is limited to the form of magnetite (Fe_3O_4). Nevertheless, if the Fe-based oxygen carriers include Al_2O_3 as support material, $FeAl_2O_4$ can be formed as a reduced compound and also achieve complete combustion of gas to CO_2 and H_2O [14-17]. Thus, the oxygen transport capacity of the oxygen carrier is increased three times in comparison with the Fe_2O_3-Fe_3O_4 redox couple. Furthermore, Fe-based oxygen carriers present a low tendency to carbon deposition [18] and no risk of sulphide or sulphate formation at any concentration or operating temperature when H_2S-containing gases are used as fuels

[17, 19-20].

Fe-based oxygen carriers have traditionally presented lower reactivity with fuel gases compared to Ni-, Cu-, and Mn-based oxygen carriers, mainly for reduction with CH_4. Consequently, incomplete combustion of CH_4 occurred in different continuous CLC plants when Fe-based materials were used [21-28]. Among these materials there were synthetic oxygen carriers prepared by different methods [21-23], iron-containing minerals [24-27] and residues [27-28]. Our research group at Instituto de Carboquímica (ICB-CSIC) has recently developed a highly reactive Fe-based oxygen carrier prepared by the impregnation method [16]. This material showed complete combustion of CH_4 during continuous operation in a 0.5 kW_{th} CLC unit [16]. Additionally, it presented adequate resistance to agglomeration and attrition, even when H_2S was present in the gas fuel at very high concentrations [17,19-20].

Process modelling is a powerful tool with which to design and optimize a CLC unit. A proper model of the fuel and air reactors in a CLC system must take into consideration the oxygen transport capacity and the reaction kinetics of the oxygen carrier particles. Kinetic determination of redox reactions becomes crucial for the simulation, design and optimization of CLC units because the solids inventory needed in the fuel and air reactors is directly related to oxygen carrier reactivity [29]. Moreover, oxygen transport capacity greatly affects the solids recirculation rate needed between the fuel and the air reactors.

Several works deal with the kinetic determination of reduction and oxidation reactions between oxygen carriers and common gases used for CLC, i.e., CH_4, CO, H_2 and O_2. Table 1 shows a summary of the research works found in the literature regarding kinetic data determined for Fe-based oxygen carrier particles. This table includes information

related to the composition of the oxygen carriers, method of preparation, properties of the evaluated materials, experimental conditions studied, and the type of reactor and model used to determine the kinetic data. The existence of different conditions inside the fluidized beds makes it essential to determine the reaction rates for a wide range of temperature and fuel concentration values. Furthermore, it is also important to calculate kinetic data for all relevant gases, i.e. CH_4, CO, H_2 and O_2, and Fe-based redox systems applicable for CLC process, such as Fe_2O_3-Fe_3O_4, Fe_2O_3-$FeAl_2O_4$ and Fe_2TiO_5-$FeTiO_3$. From the analysis of the data collected in Table 1, it can be concluded that most of the works produced to date do not provide sufficient information with which to model a CLC system using an Fe-based material as an oxygen carrier. Theoretical kinetic studies, relevant from a basic-science point of view, have been also conducted to investigate the mechanisms of interaction between reacting gases and Fe-based oxygen carriers [39-48], suggesting that the Fe_2O_3-support interaction influences material reactivity. However, these works do not provide enough practical information for CLC system design and simulation.

The aforementioned Fe-based material [16] can be considered a promising oxygen carrier for use during the scale-up of the CLC process. Therefore, determination of kinetic data would be essential in order to design, optimize and scale-up a CLC system based on this oxygen carrier. CH_4, CO and/or H_2 are considered major components in natural gas, syngas and PSA-off gas. Thus, the objective of this work was to determine the kinetic parameters for the reduction of the highly reactive Fe-based oxygen carrier with CH_4, CO and/or H_2, as well as the kinetics of oxidation with O_2. The effect of both temperature and gas concentration on reaction rate was evaluated. Moreover, the obtained parameters were further used to estimate the recirculation rate and the solids

inventory needed in a CLC system.

2. Material and methods

2.1. Oxygen carrier

A kinetic study of redox reactions for CLC was conducted for a promising Fe-based oxygen carrier prepared at ICB-CSIC. This oxygen carrier was prepared by the incipient impregnation method and was composed of Fe_2O_3, as active material, supported on γ-Al_2O_3. A detailed description of the method of preparation can be found elsewhere [16]. The total Fe_2O_3 content in the particles used in this work was 20 wt%. The main physicochemical properties of the oxygen carrier particles are shown in Table 2. This oxygen carrier is hereafter referred to as Fe20γAl.

2.2. Characterization techniques

Different techniques were used to physically and chemically characterize fresh particles of the Fe20γAl material. The total Fe_2O_3 content was determined by inductively coupled plasma atomic emission spectroscopy (ICP-AES) with a Jobin Ybon 2000 spectrometer. The mean particle size was measured by means of size particle distribution, via laser diffraction technique, according to the ISO 13320 Standard with LS 13 320 Beckman Coulter equipment. The skeletal density of the particles was determined with a Micromeritics Model AccuPyc II 1340 helium pycnometer. A Shimpo FGN-5X apparatus was used to measure the crushing strength of particles as the force needed to fracture them. Crushing strength was obtained as the average value of at least 20 measurements for particles with a particle size range of d_p = +200-400 μm. Porosity was measured by Hg intrusion in a Quantachrome PoreMaster 33, whereas the specific surface was determined by the Brunauer-Emmett-Teller (BET) method by adsorption/desorption of nitrogen at 77 K in a Micromeritics ASAP-2020

(Micromeritics Instruments Inc.). Crystalline chemical species were identified by powder X-ray diffraction (XRD) in a Bruker AXS D8 Advance system, with Bragg−Brentano geometry configuration, Cu Kα radiation and equipped with secondary graphite monochromator. Finally, the reducibility of the Fe-based oxygen carrier particles was determined by temperature-programmed reduction (TPR) experiments in an AUTOCHEM II flow apparatus from Micromeritics. In the TPR technique, the temperature was increased from room temperature to 1273 K at a constant rate of 7 K min^{-1} with a flow of 20 ml min^{-1} of a 10 vol% H_2/90 vol% Ar mixture.

2.3. Experimental setup and procedure

The kinetics of reduction and oxidation reactions with the Fe-based oxygen carrier was determined from experiments at atmospheric pressure in a TGA, CI Electronics type, described elsewhere [37]. Three different gases were used as reducing agents, i.e., CH_4, CO and H_2, whereas O_2 was used for the oxidation reactions. In all cases, the redox agents were diluted in N_2.

The samples of approximately 50 mg of oxygen carrier were loaded in a platinum basket, and a gas flow of 25 LN/h was fed into the reactor of the TGA system. External and interparticle diffusion have low relevance under these conditions [14]. Furthermore, García-Labiano et al. [49] found that oxygen carrier particles can be considered isotherm under usual operating conditions, and that mass transfer inside them is negligible.

The oxygen carrier particles were heated to the operating temperature in an air atmosphere. When the sample weight was stabilized, the oxygen carrier was exposed to a reduction and an oxidation cycle. In order to prevent the mixing of fuel and air, a 2-minute flow of N_2 was fed between the reducing and oxidizing period. This material

showed excellent stability in redox reactivity over hundreds of cycles [17]. Data obtained during the first redox cycle were selected for kinetic determination.

Different fuel gas (CH_4, CO and H_2) concentrations ranging from 5 to 60 vol% were used to determine the kinetics of the reduction reaction. In order to prevent carbon deposition, 20 vol% of H_2O or CO_2 were added to the reacting mixture when CH_4 or CO were used as fuel gases, respectively. To analyse oxidation reactivity, it was initially necessary to reduce the sample to $FeAl_2O_4$, simulating the behaviour expected in a CLC process when iron oxide (Fe_2O_3) supported on Al_2O_3 is considered as the oxygen carrier. In this case, as mentioned in the introduction section, it was possible to reach complete fuel combustion to CO_2 and H_2O, obtaining $FeAl_2O_4$ as the reduced form of the oxygen carrier. For this reason, the previous reducing periods were conducted at 1223 K in a 15 vol% CO + 20 vol% CO_2 (N_2 to balance) atmosphere. Under these conditions and with the addition of CO_2, the reduction of Fe_2O_3 was stopped at $FeAl_2O_4$, and no further reduction to metallic iron was produced. This fact was also confirmed by XRD analysis of reduced samples. The oxygen carrier particles were subsequently ready to be subjected to the oxidizing period. The O_2 concentration for oxidation was varied from 5 to 21 vol%.

To study the effect of the temperature on reduction and oxidation reaction rates, this parameter was varied between 973 and 1323 K. When the reduction reaction was studied, the fuel gas concentration was always 15 vol% and the samples were oxidized at 1223 K in an air atmosphere. On other hand, in order to evaluate the influence of temperature on oxidation kinetics, a 10 vol% O_2 concentration was always used and, as mentioned above, the reducing period was conducted at 1223 K in a 15 vol% CO + 20 vol% CO_2 (N_2 to balance) atmosphere.

2.4. Data evaluation

The following reactions took place between Fe_2O_3 and the reducing gases:

$$4\ Fe_2O_3 + 8\ \gamma\text{-}Al_2O_3 + CH_4 \Leftrightarrow 8\ FeAl_2O_4 + 2H_2O + CO_2 \quad \Delta H_{red}^{1223K} = -348.7\ \text{kJ/mol} \quad (1)$$

$$Fe_2O_3 + 2\ \gamma\text{-}Al_2O_3 + H_2 \Leftrightarrow 2\ FeAl_2O_4 + H_2O \quad \Delta H_{red}^{1223K} = -135.5\ \text{kJ/mol} \quad (2)$$

$$Fe_2O_3 + 2\ \gamma\text{-}Al_2O_3 + CO \Leftrightarrow 2\ FeAl_2O_4 + CO_2 \quad \Delta H_{red}^{1223K} = -168.1\ \text{kJ/mol} \quad (3)$$

As can be observed, all the reduction reactions were exothermic at 1223 K, a usual operating temperature for the CLC process.

For the oxidation of $FeAl_2O_4$, the following reaction was expected:

$$4\ FeAl_2O_4 + O_2 \Leftrightarrow 2\ Fe_2O_3 + 4\ \gamma\text{-}Al_2O_3 \quad \Delta H_{ox}^{1223K} = -227.1\ \text{kJ/mol} \quad (4)$$

The conversion of solids, X_S, was calculated with Eqs. (5) and (6) for the reduction or oxidation period, respectively.

$$X_{S,red} = \frac{m_{ox} - m}{m_{ox} - m_{red}} = \frac{m_{ox} - m}{R_{OC} \cdot m_{ox}} \quad (5)$$

$$X_{S,ox} = \frac{m - m_{red}}{m_{ox} - m_{red}} = 1 - \frac{m_{ox} - m}{R_{OC} \cdot m_{ox}} \quad (6)$$

where m is the actual mass of the sample, m_{red} the mass of reduced sample, m_{ox} the mass of oxidized sample. The difference between m_{ox} and m_{red} is the maximum amount of oxygen that can be transferred from the oxygen carrier to the fuel, which is defined by the oxygen transport capacity, R_{OC}. In the case of iron materials, this amount of oxygen depends on the final oxidation state during the reduction reaction. In this kinetic study, the amount of oxygen that could be provided by the oxygen carrier material to allow complete combustion of fuel to CO_2 and H_2O was considered to correspond to the reduction from hematite (Fe_2O_3) to iron aluminate ($FeAl_2O_4$) [9]. Therefore, the conversion of solids and, consequently, the reduction and oxidation kinetics were

calculated by taking this redox couple as a reference.

3. Results

3.1. Analysis of Fe_2O_3 reduction to $FeAl_2O_4$

Prior to conducting the kinetic study of this oxygen carrier, evaluation was made of what would be the most appropriate method for kinetic determination. There are mainly two methods for kinetics determination, known as the isothermal method and non-isothermal method. In this sense, different experiments for reduction reaction were carried out in a TGA system either at a fixed temperature or by TPR. From a TPR profile, see Fig. 1, three hydrogen consumption peaks were well identified at 683, 985 and 1132 K, respectively. These three peaks corresponded to the following reducing transitions: $Fe_2O_3 \rightarrow Fe_3O_4 \rightarrow FeO \rightarrow Fe$ [17]. None of these peaks could be attributed to the reduction of $FeAl_2O_4$ since the peak corresponding to the reduction from $FeAl_2O_4$ to Fe^0 would have been detected at a higher temperature [17].

In order to analyse the reduction pathway under relevant conditions in CLC, isothermal experiments were conducted at 1223 K with a reducing gas mixture of 5 vol% H_2, 48 vol% H_2O (N_2 to balance). The reduction period was stopped at different times during the operation in order to obtain several degrees of solid conversion. The corresponding samples were further subjected to XRD analyses with the aim of observing the crystalline iron phases at different degrees of oxygen carrier reduction. In all cases, the XRD technique revealed that the only Fe-based reduced phase found in the oxygen carrier was iron aluminate, $FeAl_2O_4$ together with unreacted Fe_2O_3, regardless of the degree of the oxygen carrier reduction. This result was also corroborated by thermodynamic analyses carried out with HSC Chemistry 6.1 software [50]. Moreover, tests performed with this material in a continuous CLC unit for CH_4 combustion

revealed the presence of $FeAl_2O_4$ in the oxygen carrier particles extracted from the fuel reactor as the only reduced compound [16, 17].

With the above experimental data, it can be concluded that different results regarding the reduction mechanism were found depending on the method selected for kinetic determination. However, the isothermal method, based on the experiments carried out in the TGA at a fixed temperature, provided a better fit with the conditions found in the CLC process. In this respect, it was concluded that the isothermal method was suitable to determine reaction kinetics of this material for use under typical conditions in CLC.

It was also concluded that the reduction reaction mechanism was based on the interaction of Fe_2O_3 with Al_2O_3 in presence of the reacting gases to form $FeAl_2O_4$ as the only stable Fe-based phase. Thus, as previously mentioned, the conversion of solids and, consequently, the reduction and oxidation kinetics were calculated taking the Fe_2O_3 (Al_2O_3) - $FeAl_2O_4$ redox couple as a reference.

3.2. Isothermal analysis of reduction reaction

The reduction kinetics of the Fe20γAl oxygen carrier was studied in a TGA by using three different fuels: CH_4, H_2 and CO. The kinetics were determined in a wide range of temperatures (from 973 to 1323 K) and gas concentrations (from 5 vol% to 60 vol%) typically found in a CLC unit.

3.2.1. Effect of fuel type

Fig. 2 shows the conversion vs time curves for the three fuel gases used to determine reduction kinetics. The reduction tests with H_2 and CH_4 were performed by adding 20 vol% H_2O to the reacting mixtures, whereas 20 vol% of CO_2 was added for TGA tests with CO. As can be observed, the reduction rate was very high in the three cases up to a solid conversion value of 0.6. Beyond this point, the oxygen carrier presented a slightly

different behaviour depending on the reducing gas being considered. In the cases of H_2 and CH_4, the reaction rate decreased rapidly, continuing at a very slow rate from this point. Consequently, complete reduction from Fe_2O_3 to $FeAl_2O_4$ was not achieved using these reacting agents. However, when CO was considered as the reducing gas, the reaction rate was also considerably reduced at conversion values higher than 0.6, but it was still high enough to completely reduce the oxygen carrier to $FeAl_2O_4$ after 600 s. At that point, the reduction reaction stopped and no further reduction to metallic iron took place, even though the experiment in the TGA was prolonged until 3600 s. A remarkable result obtained from the reduction tests with CO is that the active iron oxide content calculated from the TGA tests coincides accurately with the theoretical content derived from the preparation method for the oxygen carrier, i.e. the incipient impregnation method, as well as with the corresponding content determined from ICP-AES analysis, see Table 2. The haematite (Fe_2O_3) content of the oxygen carrier particles was 20 wt% in all three cases. These results mean that reduction tests in a TGA using a mixture of CO and CO_2 as reacting gas can be considered an additional, valid method to determine the mass percentage of active iron oxide in an Fe-based oxygen carrier supported on alumina. Reduction with H_2 gave a value of 15 wt% Fe_2O_3 [16], which corresponded to the fraction of Fe_2O_3 that was highly reactive.

3.2.2. Effect of gas products on the reduction reaction

Different gas products can be formed during the combustion process of a gaseous fuel, of which CO_2 and H_2O are the most relevant. The presence of different amounts of these products on the reaction atmosphere could affect the reaction rate. In order to evaluate the effect of H_2O on the reduction reaction rate of the Fe20γAl oxygen carrier, several tests were carried out with H_2 acting as reducing gas and by varying the H_2O/H_2 ratio

from 0 to 10 approximately. Fig. 3a illustrates the reduction conversion obtained for this material with H_2 when the H_2O content was varied from 0 to 48 vol.%. When H_2O was not added to the reducing gas mixture, the oxygen carrier was reduced beyond $FeAl_2O_4$, although it could not be completely reduced to metallic iron. When H_2O was added to the reducing gas, the reaction rate stopped after 50 s of reduction at a solids conversion of 0.75 approximately. A further increase in the amount of H_2O slightly changed the oxygen carrier reactivity and the reaction rate with H_2. This means that the reduction of $FeAl_2O_4$ to Fe^0 is prevented if H_2O is present in the reducing gas mixture.

On the other hand, Fig. 3b shows the conversion vs time curves obtained with 5 vol% CO when the CO_2 concentration was increased from 0 to 50 vol%. In all cases, the reaction rate was very fast up to a solids conversion value of 0.75 approximately. This degree of conversion was obtained after 30 s of reduction reaction. For higher times, the reaction rate was considerably decreased, but the oxygen carrier particles were able to be reduced completely to $FeAl_2O_4$. When CO_2 was not added to the reducing gas mixture, the oxygen carrier was reduced beyond $FeAl_2O_4$. When CO_2 was added together with the reducing gas, the behaviour of the oxygen carrier was practically the same, regardless of the CO_2 concentration used. Thus, the reduction reactivity with CO was hardly affected when the amount of CO_2 was varied from 10 to 50 vol% in the reaction gas mixture.

From the results obtained in this section it can be concluded that the presence of different concentrations of H_2O and CO_2, the main products of the combustion reaction, in the reacting gas mixtures affected neither the reaction rate nor the reactivity of the oxygen carrier. Only the avoidance of these gases in the reaction gas mixture increased the reaction rate during the reaction at high solids conversion values, characterized by

slow reactivity. However, H_2O and CO_2 are considered to be in the gas reacting in the fuel reactor because they would be quickly generated in the fuel reactor, or can even be present in fluidizing gases, e.g. in the fuel gas itself or in gases introduced into loop seals. Therefore, kinetic determination was obtained considering the presence of H_2O or CO_2 in the reacting gas mixture.

3.2.3. Effect of gas concentration

The concentration of fuel gases inside a fuel reactor varies with height along the fluidized bed. The oxygen carrier is usually in contact with high fuel concentration values at the bottom, whereas the concentration of fuel gases decreases dramatically at the top of the bed in such a way that the gaseous mixture is mainly composed of CO_2 and H_2O.

The effect of fuel gas concentration on the reduction of the Fe20γAl oxygen carrier was determined by carrying out experiments in a TGA with different concentrations of CH_4, CO and H_2 at a temperature of 1223 K. In the cases of CH_4 and H_2, the fuel gas concentration was varied from 5 to 30 vol%, while the concentration of CO was increased up to 60 vol%. The conversion vs time curves corresponding to the three fuel gases are shown in Fig. 4 (a-c). An increase in the reaction rate was noticed during the first part of the reduction period as the fuel gas concentration was increased. At the beginning of the period, the reaction rate was very fast for all the fuel gases (for 10 s for CH_4 and H_2 and for 20 s for CO, respectively), however it decreased immediately, continuing at a very low rate for the rest of the period. In this second period, characterized by a low reaction rate, the fuel gas concentration barely affected the reduction rate of the oxygen carrier with the different fuel gases. This behaviour indicates that the corresponding reduction reactions are controlled by two different

resistances. The change in controlling mechanism happens at conversion values of 0.45 for CH_4 and H_2 and at 0.7 for CO.

3.2.4. Effect of temperature

The effect of temperature on the reduction reactivity of the Fe20γAl oxygen carrier was also evaluated. In this case, the concentration of the reducing gases for these tests was set at a fixed value and the temperature was varied from 973 to 1323 K. This range of values includes the usual operating temperatures in a CLC system. Fig. 5 (a-d) shows solids conversion as a function of time for the following reducing gas mixtures: (a) 15 vol% CH_4 + 20 vol% H_2O; (b) 15 vol% CO + 20 vol% CO_2; (c) 15 vol% H_2 + 20 vol% H_2O; and (d) 5 vol% H_2 + 48 vol% H_2O. The gas mixtures were completed with N_2 in all four cases. The reaction rate and final reduction conversion of the oxygen carrier were affected by the temperature, since an increase in this parameter produced an increase in both terms. In the case of the final conversion reached for the oxygen carrier this means that the reduction degree to iron aluminate ($FeAl_2O_4$) was clearly influenced by the temperature.

Solids conversion was quite low at T < 1073 K, mainly for CH_4 and H_2, but the reaction rate was relatively fast during the first seconds of the reduction period when $X_{S,red} < 0.2$. As in the case of the study of the effect of gas concentration (see Section 3.2.3), this behaviour indicates that the reducing reaction is controlled by two different resistances depending on solids conversion. At low $X_{S,red}$ values, the reaction rate was fast. However, as the oxygen carrier particles were reduced to a greater extent, the control step changes and the reaction rate quickly decreased. The same behaviour was observed at higher temperatures for all the reducing gases, with the difference that the reduction conversion at which the reaction rate changed from fast to slow increased with

temperature. This fact was the main reason for the increase in conversion achieved at long times with temperature. The effect of temperature on the reaction rate during the second step, which was characterized by a low reaction rate, was low. This fact can be seen because the conversion vs time curves obtained at different temperatures were practically parallel.

3.3. Isothermal analysis of oxidation reaction

Oxidation of the oxygen carrier takes place in the air reactor. Fully or partially reduced particles coming from the fuel reactor are exposed to air in the air reactor with the aim of regenerating the material for a new reduction step. Different O_2 concentrations exist in the air reactor. The O_2 concentration varies along the bed height from 21 vol% to the O_2 concentration in the exhaust air stream. An O_2 concentration of 4 vol% at the top of the bed, a typical value in a CLC plant [51], is equivalent to 20% excess air in the air reactor. Therefore, the concentration in the studies using the TGA was varied between 5 and 21 vol% O_2 (N_2 to balance), and the temperature from 1073 to 1273 K. The experiments were carried out following the procedure described in the experimental section.

3.3.1. Effect of O_2 concentration

Fig. 6 illustrates the conversion of the oxygen carrier during oxidation at 1223 K with 5, 10, 15 and 21 vol.% O_2. The oxidation reaction rate increased as the O_2 concentration was increased. These conversion vs time curves evidence the high speed at which the oxidation reaction took place. The oxygen carrier samples were fully oxidized in all cases and the time for complete conversion ranged between 15 s and 50 s.

3.3.2. Effect of temperature on the oxidation reaction

The effect of the temperature on the oxidation reaction was also investigated in this work. The influence of this parameter was studied between 1073 and 1273 K. Fig. 7 shows solids conversion as a function of time for an O_2 concentration of 10 vol%. In this case the variation in temperature scarcely affects the reaction rate. As in the previous case (see Section 3.2.1), the oxidation reaction was very fast and the samples were always fully oxidized at the end of the oxidation period.

3.4. Kinetic model

The kinetic parameters of the reduction and oxidation reactions can be determined using a particle reaction model that fits adequately with the experimental results. For materials prepared by impregnation, the grain model with uniform conversion in the particle and reaction in grains following shrinking core model [52]. From previous Figures (Figs. 3-7), some information was acquired regarding the mechanisms controlling the reduction and oxidation reactions with the Fe20γAl oxygen carrier. The reaction rate was observed to be very fast with all gases at the beginning of the reduction period. However, it decreased immediately and continued at a very low rate for the rest of the period. This behaviour indicates that the corresponding reduction reactions are controlled by two different resistances. Furthermore, it should be taken into account that magnetite (Fe_3O_4) never appears as the Fe-based reduced phase and $FeAl_2O_4$ was the only reduced compound in the presence of H_2O or CO_2 when the oxygen carrier was reduced by H_2 or CO_2, respectively.

Fig. 8, is a schematic illustration of the proposed reacting mechanism for CH_4 reduction with the Fe20γAl oxygen carrier. The reacting model for reduction kinetics assumes a first step with the reaction rate controlled by chemical reaction in the grain surface [53-54]. During this first step, alumina and oxygen must diffuse towards the reaction

interphase. As a result, a product layer of $FeAl_2O_4$ is formed. In the second step, the mechanism that controls the reaction at higher conversion values is the diffusion through the product layer of $FeAl_2O_4$ around the grains. Moreover, the reduction rate during this step is independent of the fuel gas concentration. This fact suggests that diffusion of the reacting gas is blocked, but oxygen must diffuse outwards [53]. Thus, chemical reaction still takes place on the grain surface, but the reaction rate is now limited by oxygen diffusion through the product layer. A third step, based on the reaction of $FeAl_2O_4$ with H_2 or CO in a highly reducing atmosphere to form metallic iron, was not considered for the reacting model since this step must not take place in a CLC process if complete combustion of the fuel gas is desired, because of thermodynamic restrictions for H_2 or CO conversion when $FeAl_2O_4$ is reduced to Fe^0 [9].

Taking the above comments and conditions in the TGA into consideration, the dependence of solids conversion with time for this Fe-based oxygen carrier is described by the following equation [55]:

$$t = \tau_{ch} \cdot X_{S,red} + \tau_{pl}\left(1 - 3\left(1 - X_{S,red}\right)^{2/3} + 2\left(1 - X_{S,red}\right)\right) \quad (7)$$

where τ_{ch} and τ_{pl} are the times for complete reduction conversion of the particle owing to the chemical reaction and the diffusion through the product layer. τ_{ch} is calculated as follows:

$$\tau_{ch} = \frac{1}{k_s \cdot C_i^n} \quad (8)$$

where k_s is the chemical kinetic constant, which follows an Arrhenius-type expression with temperature:

$$k_s = k_{s,0}\, e^{\frac{-E_{ch}}{R_g \cdot T}} \tag{9}$$

The time of complete conversion for the diffusion through the product layer reaction, τ_{pl}, is defined by expression (10):

$$\tau_{pl} = \frac{1}{D_{pl} \cdot C_i^{n'}} \tag{10}$$

In this experimental work, a sharp decrease in the reaction rate over time was observed when the diffusion through the product layer of $FeAl_2O_4$ controlled the reduction reaction. This suggests that the effective product layer diffusivity, D_{pl}, is affected both by temperature and solids conversion. In this case, an additional term to the effect with temperature is included, which modifies the effective diffusivity through the product layer [56-57], with D_{pl} calculated as:

$$D_{pl} = D_{pl,0}\, e^{-k_X \cdot X_{s,red}} e^{\frac{-E_{pl}}{R_g T}} \tag{11}$$

where

$$k_X = k_{X,0}\, e^{\frac{-E_X}{R_g \cdot T}} \tag{12}$$

With regard to oxidation kinetics, the reacting model assumes a reaction rate only controlled by chemical reaction, since the reaction rate was very fast for the complete conversion of the oxygen carrier. The dependence of oxidation conversion on time for this Fe20γAl oxygen carrier is described by the following equation:

$$t = \tau_{ch} \cdot X_{S,ox} \tag{13}$$

3.5. Determination of kinetic parameters

The kinetics parameters for reduction with CH_4, H_2, CO and oxidation with O_2 were calculated with the kinetic model presented in the previous section.

In a first stage, the kinetic parameters corresponding to the case where the reaction rate is controlled by the chemical reaction in the gas-solid interphase were determined. Thus, the first step of the reaction is described by the following equation:

$$t = \tau_{ch} \cdot X_S \tag{14}$$

τ_{ch} values are obtained at different C_i by fitting each experimental curve. Thus, the following equation was deduced from expression (8).

$$\ln\left(\frac{1}{\tau_{ch}}\right) = \ln k_s + n \cdot \ln C_i \tag{15}$$

Fig. 9 shows a plot of ln(C_i) vs ln ($1/\tau_{ch}$) in order to calculate the reaction order, n, with respect to each reducing or oxidizing agent. This parameter was obtained for each gas from the slope of each curve. Furthermore, the chemical kinetic constant, k_s, could be obtained from the intercept. The reaction order calculated for reduction with CH_4 and oxidation with O_2 were the lowest and the highest, respectively. The reaction order for reduction with CH_4 was very similar to that obtained by Mogthaderi and Song [34] with a Fe-based oxygen carrier supported on Al_2O_3 and prepared by mechanical mixing using the shrinking core model (SCM) for kinetic determination. In the case of reduction with H_2 and CO, these authors found values that were considerably higher. With regard to oxidation reaction, Abad et al. [29] determined a reaction order of 1 with O_2 using a Fe-based oxygen carrier prepared by freeze granulation, which is a value very similar to the one found in this work.

By fitting the conversion vs time curves in Figs. 5 and 7 with the model, parameter k_s was determined at each temperature. The Arrhenius plot obtained from the reduction and oxidation reactions is shown in Fig. 10 (a). From the slope of the curves, the activation energy, E_{ch}, was determined for each reaction. The highest value was

obtained for CH_4, i.e., 66 kJ/mol, whereas the activation energies for H_2, CO and O_2 were considerably lower, ranging from 8 to 23 kJ/mol. The value of the activation energy for oxidation reaction, i.e., 23 kJ/mol, was higher in comparison with other kinetic studies conducted in the literature on Fe-based oxygen carriers [21,29,36]. The opposite behaviour was found with the activation energies for reduction reactions with CO and H_2. In these cases, the values determined in this work were slightly lower than the ones found in the literature, see Table 1.

As mentioned previously, diffusion through the product layer became the limiting step that controlled the reduction reactions at higher solids conversion values. The corresponding kinetic parameters fitting the conversion curves for different gas concentrations and temperatures were also calculated.

It was found that the reacting gas concentration had no influence over the diffusion mechanism. Furthermore, it was observed that the decay constant, k_X, was not dependent on the reacting temperature since there were no perceptible variations in the slope of the conversion vs time curves when the reaction rate was controlled by the diffusion mechanism. It should be noted that parameter k_X affects the intensity of the reaction rate decrease in the second step, which was similar at all temperatures tested in this work. Therefore, the activation energy for k_X was considered to be $E_X = 0$ J mol^{-1}.

Fig. 10 (b) illustrates a plot of ln (D_{pl}) vs the inverse of the temperature in order to determine the pre-exponential factor, $D_{pl,0}$, and the activation energy, E_{pl}, for the reduction reactions. Both parameters achieved the highest values for CH_4 reduction, see Table 3. Finally, the decay constant, k_X, was also calculated. This parameter took the highest value for the reduction reaction with CH_4, since the decrease in the reaction rate with time was slightly more noticeable with this gas than with the other reducing gases.

Table 3 shows the kinetic parameters obtained in this work for reduction of Fe20γAl material with CH_4, H_2 and CO, as well as for oxidation with O_2.

As can be observed in Figs. 4-7, the theoretical curves determined from the reaction model correctly predicted the experimental results obtained during the whole reacting time for each type of gas, temperature and concentration considered.

4. Discussion

The reaction kinetics and oxygen transport capacity determined in this work can be used to evaluate relevant parameters for the design of a CLC system, such as the solids circulation rate between the fuel reactor and the air reactor and the solids inventory in both reactors.

The solids circulation rate must be high enough to transfer oxygen for fuel combustion and to provide the heat necessary to maintain optimum temperatures in the system. In the case of an Fe-based oxygen carrier supported on Al_2O_3 for which the Fe_2O_3/Al_2O_3 - $FeAl_2O_4$ redox couple is considered, heat plays a less important role because both reduction and oxidation reactions are exothermic [9]. Thus, there are no restrictions on the solids circulation rate in order to maintain a low temperature difference between both reactors [29].

In a previous work, Abad et al. [29] developed a simplified model to determine the solids inventory and the solids circulation rate in a CLC system taking into consideration the reactivity and oxygen transport capacity of the oxygen carrier particles. This method enables the magnitude order of the design parameters to be established and, therefore, a comparison between oxygen carriers can be made by analysing the obtained values.

4.1. Solids recirculation rate

The solids circulation rate depends on the oxygen carrier and the fuel used, as well as on the variation of solids conversion in the fuel reactor and air reactor. As previously mentioned, the recirculation rate was calculated according to the model developed by Abad et al. [29]. This parameter is defined by Eq. (16), expressed as the mass flow of fully oxidized oxygen carrier material, taking as a reference the 1 MW_{th} of power provided by the fuel and assuming complete gas conversion (ΔX_g =1).

$$\dot{m}_{OC} = \frac{\dot{m}_c}{\Delta X_s} \tag{16}$$

where $\dot{m}_c$ is the characteristic circulation rate, a specific parameter for each oxygen carrier-fuel combination.

$$\dot{m}_c = \frac{2 \cdot d \cdot M_O}{R_{OC} \cdot \Delta H_C^0} \tag{17}$$

The oxygen transport capacity of the material, R_{OC}, is defined as $R_{OC} = R_O \cdot x_{MeO}$, where x_{MeO} is the mass percentage of metal oxide in the oxygen carrier. The active Fe_2O_3 content in the oxygen carrier was 20 wt% and $R_O = 10\ \%$ for the Fe_2O_3-$FeAl_2O_4$ redox couple. Thus, the oxygen transport capacity was R_{OC} = 0.02. The $\dot{m}_c$ parameter took values of 4.0, 3.3 and 2.8 kg s^{-1} MW^{-1} for this material when considering CH_4, H_2 and CO as fuels, respectively.

Fig. 11 illustrates the circulation rate, $\dot{m}_{OC}$, as a function of the variation of solids conversion in the fuel reactor if CH_4 is used for reduction reaction. The solids circulation rate in a CLC unit is often evaluated by using the oxygen carrier to fuel ratio, ϕ, which expresses the molar ratio between the potential flow oxygen in circulating oxygen carrier and the required flow of oxygen for fuel combustion. Thus, the ϕ

parameter is also included in Fig. 11. It can be observed that $\dot{m}_{OC}$ parameter decreased as the variation of solids conversion, ΔX_s, increased. The minimum circulation rate for CH_4 combustion with the Fe20γAl oxygen carrier at $\Delta X_s = 1$ was 4.0 kg s^{-1} MW^{-1}. On the other hand, the solids circulation flow was dependent on the operating conditions and the configuration of the riser in the CLC unit. For usual conditions of velocity, temperature and excess of air, the maximum circulation rate in a CLC system is established at 16 kg s^{-1} MW^{-1} [29]. Therefore, a solids conversion higher than 0.25 would be necessary for this material in order to maintain the flow of solids under the average maximum limit of 16 kg s^{-1} MW^{-1} if CH_4 is used as the feed gas for the CLC unit.

Furthermore, it must be taken into consideration that temperature greatly affected the reduction conversion degree of the oxygen carrier, and, consequently, the solids circulation rate. It can be inferred from Fig. 5 that, depending on the operating temperature in the CLC system, the maximum variation of reduction conversion reached by this material in the fuel reactor would be different. As a first approximation, it was assumed that the oxygen carrier would only be reduced in a real CLC system up to solids conversion values within the range at which the reaction kinetics was controlled by chemical reaction. Therefore, the maximum variation of reduction conversion was determined from experimental results for the different reacting gases in a usual range of operating temperatures, see Fig. 12. From the results shown in Figs 11 and 12, important conclusions regarding adequate operating temperatures in the fuel reactor and solids circulation rates in the CLC system can be deduced if the Fe20γAl material is used as an oxygen carrier. For CH_4 combustion, it was concluded that $\Delta X_s <$ 0.25 would not be allowed if a maximum limit of 16 kg s^{-1} MW^{-1} were assumed [29].

Therefore, temperatures lower than 1100 K could not be used in the fuel reactor since the maximum variation of reduction conversion reached at this temperature (see Fig. 12) would require a solids circulation rate higher than the upper limit. On the contrary, at temperatures higher than 1273 K, the corresponding values of $\Delta X_{S,ch}$ and solids circulation rate were 0.57 and 7.0 kg s^{-1} MW^{-1} respectively.

4.2. Solids inventory

In a CLC process, it is desirable to minimize the amount of oxygen carrier existing in the fuel and air reactors in order to reduce the size of the plant fan power and the cost relative to the oxygen carrier. The solids inventory can be determined from a mass balance to the oxygen carrier and fuel gas in both reactors in combination with reaction kinetics. Furthermore, the solids inventory is also directly related to the reactivity and oxygen transport capacity of the oxygen carrier.

As in the case of the determination of the solids circulation rate, the calculation of the solids inventory was also based on the methodology developed by Abad et al. [29]. The solids inventory in the fuel reactor and air reactor, $m_{OC,FR}$ and $m_{OC,AR}$, can be expressed according to Equations (18) and (19):

$$m_{OC,FR} = \dot{m}_c \frac{\tau_r}{\Phi_{FR}} \tag{18}$$

$$m_{OC,AR} = \dot{m}_c \frac{\tau_o}{\Phi_{AR}} \tag{19}$$

where τ_r and τ_o are the times for complete conversion of the particles in the fuel reactor and air reactor, respectively. These parameters are obtained at an average reacting gas concentration calculated from the following expression:

$$\overline{C}_i = \frac{\Delta X_g \cdot C_{i,0}^n}{\int_{Xg,in}^{Xg,out} \left[\frac{1+\varepsilon_g \cdot X_g}{1-X_g} \right]^n dX_g} \quad (20)$$

where ε_g represents the expansion of volume as a result of the chemical reaction and can be calculated as:

$$\varepsilon_g = \frac{V_{g,X_g=1} - V_{g,X_{g=0}}}{V_{g,X_g=0}} \quad (21)$$

where $V_{g,Xg=0}$ and $V_{g,Xg=1}$ are the volumes of the gas mixture at X_g = 0 and X_g = 1, respectively. This parameter changes its value depending on the fuel gas considered for the CLC process. For example, ε_g takes a value of 2 for CH_4, 0 for H_2 and CO and −0.21 for the oxidation reaction with air.

The average concentrations were determined at 1223 K in both reactors taking into consideration the reaction order, *n*, shown in Table 3. When 100 vol% fuel gas concentration at the fuel reactor inlet and a final gas conversion of 0.999 was considered, the average CH_4, H_2 and CO concentrations in this reactor were 15.7, 30.7 and 24.6 vol%, respectively. On other hand, for an oxidation reaction in the air reactor with 21 vol% O_2 and 20 vol% excess air, the resulting average O_2 concentration was 11.2 vol%. The times for complete conversion of the particles in the fuel reactor, considering a temperature of 1223 K, were 13.7, 11.0 and 14.2 s for CH_4, H_2 and CO combustion, respectively. In the case of oxidation reaction, the time for complete conversion of the Fe20γAl oxygen carrier particles in the air reactor at 1223 K was 23.9 s.

Equations (18) and (19) are also dependent on parameters Φ_{FR} and Φ_{AR} which are the characteristic reactivity in the fuel reactor and air reactor respectively. Assuming perfect

mixing of the solids in both reactors, Φ_j can be expressed as a function of the variation of solids conversion and as a function of the solids conversion in the inlet of each reactor. For the kinetic model used in this work, the expressions for Φ_j are the following and take a value between 0 and 1:

$$\Phi_{FR} = 1 - \exp\left(- \frac{\left(1 - X_{S,red\ in\ FR}\right)}{\Delta X_S} \Phi_{FR} \right) \tag{22}$$

$$\Phi_{AR} = 1 - \exp\left(- \frac{\left(1 - X_{S,ox\ in\ AR}\right)}{\Delta X_S} \Phi_{AR} \right) \tag{23}$$

The total solids inventory in the CLC system, defined in terms of kilograms of fully oxidized oxygen carrier per MW of fuel, can be calculated adding the masses obtained in the fuel reactor and air reactor:

$$m_{OC} = m_{OC,FR} + m_{OC,AR} \tag{24}$$

For comparison purposes, the minimum solids inventory in the CLC system was calculated for the three reducing gases considered in this work, i.e., CH_4, H_2 and CO considering fuel and air reactors at 1223 K. In this case, $\Delta X_{s,red\ ch} = 0.52$, and the active Fe_2O_3 content was 10.4 wt%; see Fig. 12. Thus, $R_{OC} = 1.04$ wt%. But the reacting time to achieve the solids conversion $\Delta X_{s,red\ ch}$, i.e. $\tau_r^{'}$ to be used in Eq. (18) instead of τ_r, was conveniently reduced by (see Appendix A)

$$\tau_r^{'} = \Delta X_{s,red\ ch} \tau_r \tag{25}$$

The minimum solids inventory was obtained when the variation of solids conversion in the reactors was very low ($\Delta X_S \to 0$) and the characteristic reactivity reached the highest value. For the kinetic model used in this work, the highest value of parameter Φ_j is 1. The minimum solids inventories for CH_4, H_2 and CO combustion were 149, 116 and

109 kg MW^{-1}, respectively, see Table 4. A comparison between the expected performance of different oxygen carriers can easily be made by contrasting the minimum solids inventory values. The minimum solids inventories obtained for the Fe20γAl material were compared to the ones found for the Fe45Al oxygen carrier prepared by freeze granulation [29] or ilmenite [37]. In fact, the high reactivity of Fe20γAl with CH_4 resulted in a lower solids inventory in the fuel reactor for Fe20γAl (54 kg/MW_{th}) compared to that of Fe45Al (950 kg/MW_{th}) and of activated ilmenite (272 kg/MW_{th}), even when the iron content in these materials was higher. Thus, it can be concluded that the Fe20γAl oxygen carrier, prepared by the incipient impregnation method, presents much higher reactivity with CH_4, and hence the minimum solids inventory needed in the CLC unit reactor is lower in comparison with the other Fe-based material.

In real conditions, the solids inventory depends on the degree of oxidation of the oxygen carrier particles in the inlet of both reactors and on the value of ΔX_S. Furthermore, it must be also taken into consideration that in real conditions, the variation of solids conversion, ΔX_S, is defined by the solids circulation rate established in the CLC system, see Eq. (16), and it is possible that the oxygen carrier will not completely oxidized when it enters the fuel reactor .

Fig. 13 illustrates the total solids inventory of the Fe20γAl oxygen carrier needed in a CLC unit for CH_4 combustion as a function of the oxidation conversion of the particles at the inlet of the fuel reactor considering that the variation of solids conversion, ΔX_S, is limited to the minimum value related to the maximum solids circulation rate of 16 kg s^{-1} MW^{-1}. Thus, these calculations were made for a variation of solids conversion of 0.25, see Fig. 11. This value of ΔX_S is adequate because it is within the optimum

range proposed by Abad et al. [29], i.e., $\Delta X_S = 0.2 - 0.5$, to obtain low solids inventories and reasonable circulation rate values.

Now, the method to calculate Φ_{FR} was modified from that shown by Abad et al. [29] to consider the active Fe_2O_3 fraction as being only the fraction reacting with chemical control, but the solid fraction reacting with slow diffusional controlled reaction was assumed to be inert; see Appendix A. Thus, to calculate Φ_{FR} by Eq. (22), a modified conversion $X'_{S,\,red}$ was used, which ranges from 0 to 1 when the solids conversion varies from 0 to $X_{S,\,red\,ch}$. Considering the case of CH_4 combustion at 1223 K, $X_{S,red\,ch}$ was established at 0.52 approximately (see Fig. 12), which means that for a variation of solids conversion of $\Delta X_S = 0.25$, $\Delta X'_S$ takes a value of 0.48.

With the above considerations, the inlet conversion of solids to the fuel reactor must fulfill $X_{S,ox\,in\,FR} > \Delta X_S + \left(1 - X_{S,red\,ch}\right)$ because the fraction $\left(1 - X_{S,red\,ch}\right)$ is considered inert for the reduction reaction. It can be observed in Fig. 13 that the minimum oxidation conversion at the inlet of the fuel reactor is $X_{S,ox\,in\,FR} = 0.73$ for $\Delta X_S = 0.25$. If the value of parameter $X_{S,ox\,in\,FR}$ is very close to the aforementioned limit, the availability of oxygen for the reduction conversion will be low because the oxygen carrier particles are reduced to a great extent and, consequently, the required solids inventory in this reactor will tend towards infinity. At the same time, a low value of $X_{S,ox\,in\,FR}$ implies that the solids inventory needed in the air reactor decreases. The opposite reasoning can be made for very high values of oxidation conversion at the fuel reactor inlet. The combination of both effects over the total solids inventory entails the presence of a minimum which corresponds to the optimum solids inventory in the CLC

system under these conditions. In this case, the minimum amount of this material is 272 kg MW^{-1} at an approximated value of $X_{S,ox\ in\ FR} = 0.85$.

Finally, it should be remarked that the value of solids inventory calculated for a real CLC system would be from 2 to 10 times higher [58] because the method for determination does not take into consideration such fluidization effects as the resistance to gas exchange between the bubbles and the emulsion in the fluidized beds. For example, Gayán et al. [16] found that for this oxygen carrier a solids inventory of 500 kg MW^{-1} was necessary for complete combustion of CH_4 in the fuel reactor of a 500 W_{th} continuous CLC unit. Thus, the total solids inventory in this CLC unit would be within the range established by Abad et al. [58] taking into consideration the value calculated in this work. Therefore, these values are valid for comparison purposes with other oxygen carriers, but not for design purposes.

The results obtained from this simplified model provide valuable information for comparison purposes with different materials and a first approximation to the total solids inventory needed in a real CLC system. For example, when using this calculation method, the Fe20γAl oxygen carrier presents a much lower value of total solids inventory for CH_4 combustion in comparison with another Fe-based oxygen carrier supported on Al_2O_3 with 60 wt% Fe_2O_3 prepared by freeze granulation [29]. This fact emphasizes the high reactivity achieved by oxygen carriers prepared by means of the impregnation method. On other hand, the solids inventory obtained for the Fe20γAl material is higher than the ones found for Ni- or Cu-based oxygen carriers in that work [29]. However, it must be considered that iron is significantly cheaper and more environmentally friendly than either nickel or copper.

5. Conclusions

The isothermal method in a TGA was identified as the proper method with which to obtain the reduction and oxidation kinetics of the Fe20γAl oxygen carrier with CH_4, H_2, CO and O_2 as reacting gases under typical CLC conditions. The effect of temperature and the concentration of the reacting gases on reaction rate of Fe20γAl material were studied.

The Fe20γAl oxygen carrier was always reduced to $FeAl_2O_4$ at typical temperatures in CLC regardless of the final solids conversion achieved in the oxygen carrier samples. The formation of Fe_3O_4 as a reduced Fe-based phase was never found in the particles. This result suggested that the reduction reaction mechanism was based on the interaction of Fe_2O_3 with Al_2O_3 in presence of the reacting gases to form $FeAl_2O_4$ as the only stable Fe-based phase. Furthermore, it was found that the reduction rate and the final solids conversion were clearly affected by the temperature. Nevertheless, complete regeneration was found after the oxidation step with O_2.

The grain model with uniform conversion in the particle and reaction in grains following the shrinking core model (SCM) was used for kinetics determination, assuming a first step of reduction controlled by chemical reaction, followed by a second step controlled by the diffusion through the product layer around the grains. The reaction order values found for the reducing gases ranged between 0.25 and 0.6. Additionally, the lowest and the highest activation energy values were found for reduction reactions with H_2 and CH_4 respectively, 8 and 66 kJ/mol. With regard to oxidation kinetics, the reacting model assumed a reaction rate that was only controlled by chemical reaction. The reaction order took a value of 0.9 and the activation energy for oxidation reaction with O_2 was 23 kJ/mol.

Finally, the solids inventory needed in a CLC system was also estimated taking into consideration the results obtained from the kinetics study. Firstly, it was found that the minimum solids inventories for CH_4, H_2 and CO combustion with the Fe20γAl oxygen carrier were 149, 116 and 109 kg MW^{-1}, respectively. Furthermore, the solids inventory was calculated for usual operating conditions in a CLC unit, such as $\Delta X_s = 0.25$ and a temperature in the fuel reactor and air reactor of 1223 K. Under these conditions, and considering CH_4 as fuel gas, the minimum total solids inventory was 272 kg MW^{-1}.

Acknowledgements

This paper is based on the work carried out within the framework of the SUCCESS project, funded by the European Commission under the seventh Framework Programme (Contract 608571). This research was supported by the Spanish Ministry of Science and Innovation (MICINN Project: ENE2011-26354) and by FEDER.

Nomenclature

C_i = concentration of reacting gas i (mol m^{-3})

$\overline{C_i}$ = average concentration of gas i in the reactor (mol m^{-3})

$C_{i,0}$ = inlet concentration of gas i into the reactor (mol m^{-3})

d = stoichiometric factor in the fuel combustion reaction with oxygen (mol O_2 per mol fuel)

d_p = particle diameter (μm)

D_{pl} = effective product layer diffusivity ($m^{3n'}$ $mol^{-n'}$ s^{-1})

$D_{pl,0}$ = pre-exponential factor for effective product layer diffusivity ($m^{3n'}$ $mol^{-n'}$ s^{-1})

E_{act} = activation energy of the kinetic studies presented in Table 1 (kJ mol^{-1})

E_{ch} = activation energy for the chemical reaction (kJ mol^{-1})

E_{pl} = activation energy for the diffusion through the product layer reaction (kJ mol^{-1})

E_X = activation energy which modifies the decay constant for the product layer diffusivity (kJ mol^{-1})

F_g = shape factor for the grain

k_s = chemical kinetic constant (m^{3n} mol^{-n} s^{-1})

$k_{s,0}$ = pre-exponential factor for chemical kinetic constant (m^{3n} mol^{-n} s^{-1})

k_X = decay constant for the product layer diffusivity

$k_{X,0}$ = pre-exponential factor for decay constant for the product layer diffusivity

m = actual mass of the oxygen carrier (kg)

$\dot{m}_c$ = characteristic circulation rate (kg s^{-1} MW^{-1})

$\dot{m}_{OC}$ = circulation rate of fully oxidized oxygen carrier (kg s^{-1} MW^{-1})

m_{OC} = total solids inventory in the air reactor and fuel reactor (kg MW^{-1})

$m_{OC,j}$ = solids inventory in the reactor j (kg MW^{-1})

m_{ox} = mass of the sample of oxygen carrier when it is fully oxidized (kg)

m_{red} = mass of the sample of oxygen carrier in reduced form (kg)

M_O = molecular weight of oxygen (g mol^{-1})

n = reaction order for reacting gas in gas-solid chemical reaction

n' = exponential constant for gas concentration in the product layer diffusion process

R_g = constant for ideal gases (R_g = 8.314 J mol^{-1} K^{-1})

R_O = oxygen transport capacity of the pure metal oxide (kg oxygen per kg metal oxide)

R_{OC} = oxygen transport capacity of the oxygen carrier (kg oxygen per kg solids)

R'_{OC} = maximum oxygen transport capacity of the oxygen carrier when the reaction kinetics is controlled by chemical reaction

t = time (s)

T = temperature (K)

$V_{g,Xg=0}$ volume of the gas mixture at X_g = 0 (m^3)

$V_{g,Xg=1}$ volume of the gas mixture at X_g = 1 (m^3)

x_{MeO} = metal oxide content

X_g = gas conversion

$X_{g,in}$ = gas conversion at the reactor inlet

$X_{g,out}$ = gas conversion at the reactor outlet

X_S = conversion of solids

$X_{S,ox\ in\ AR}$ = oxidation conversion of solids at the inlet of the air reactor

$X'_{S,ox\ in\ AR}$ = normalized oxidation conversion of solids at the inlet of the air reactor when the reaction kinetics is controlled by chemical reaction

$X_{S,ox\ in\ FR}$ = oxidation conversion of solids at the inlet of the fuel reactor

$X'_{S,ox\ in\ FR}$ = normalized oxidation conversion of solids at the fuel reactor inlet when the reaction kinetics is controlled by chemical reaction

$X_{S,ox\ min}$ = minimum oxidation conversion of solids when the reaction kinetics is controlled by chemical reaction

$X_{S,red\ in\ FR}$ = reduction conversion of solids at the inlet of the fuel reactor

$X'_{S,red\ in\ FR}$ = normalized reduction conversion of solids at the fuel reactor inlet when the reaction kinetics is controlled by chemical reaction

Greek symbols:

ε = porosity of particles

ε_g = coefficient of expansion of the gas mixture

ΔH = variation of enthalpy for reduction or oxidation reactions (kJ mol^{-1})

ΔH_C^0 = standard heat of the gas fuel combustion (kJ mol^{-1})

ΔX_g = variation of gas conversion

ΔX_S = variation of solids conversion between fuel reactor and air reactor

$\Delta X'_S$ = normalized variation of solids conversion between fuel reactor and air reactor when the reaction kinetics is controlled by chemical reaction

$\Delta X_{S,red\ ch}$ = variation of solids conversion between fuel reactor and air reactor when the reaction kinetics is controlled by chemical reaction

τ_{ch} = time for complete conversion when the chemical reaction controls the process (s)

τ_o = time for complete conversion of particles in the air reactor (s)

τ_{pl} = time for complete conversion when the diffusion through the product layer controls the process (s)

τ_r = time for complete conversion of particles in the fuel reactor (s)

$\tau_r^{'}$ = time for complete conversion of particles in the fuel reactor when the reaction kinetics is only controlled by chemical reaction (s)

Φ_j = characteristic reactivity in the reactor j

$\Phi_j^{'}$ = characteristic reactivity in the reactor j when the reaction kinetics is only controlled by chemical reaction

Subscripts

i = gas (CH_4, H_2, CO)

j = reactor (AR = air reactor, FR = fuel reactor)

ox = oxidation

red = reduction

Abbreviations

CGSM: Changing Grain Size Model

CLC: Chemical Looping Combustion

SCM: Shrinking Core Model

DRM: Diffusion Reaction Model

ICP-AES: Inductively Coupled Plasma Atomic Emission Spectroscopy

MVM: Modified Volumetric Model

TGA: Thermogravimetric Analyser

TPR: Temperature-Programmed Reduction

VM: Volumetric Model

XRD: X-ray Diffraction

References

[1] IPCC, 2013. Climate Change 2013: The Physical Science Basis. Technical Summary. Working Group I Contribution to the IPCC Fifth Assessment Report (AR5).

[2] IPCC, 2005. Special report on carbon dioxide capture and storage. Working group II of the Intergovernmental Panel on Climate Change, Editors: B. Metz, O. Davidson, H. de Coninck, M. Loos, L. Meyer, Cambridge University Press, Cambridge, UK and New York, NY, USA, 2005.

[3] W.K. Lewis, E.R. Gilliland, Production of pure carbon dioxide, S.O.D Company, US Patent: 2 665 971, United States, 1954.

[4] H.J. Richter, K. Knoche, Reversibility of combustion processes. Efficiency and costing - Second law analysis of processes, ACS Symposium Series 235 (1983) 71-85.

[5] M. Ishida, D. Zheng, T. Akehata, Evaluation of a chemical-looping-combustion power-generation system by graphic exergy analysis, Energy 12 (1987) 147-154.

[6] M. Ishida, H. Jin, A new advanced power-generation system using chemical-looping combustion, Energy 19 (1994) 415-422.

[7] M. Ishida, H. Jin, A novel combustor based on chemical-looping reactions and its reaction kinetics, J. Chem. Eng. Jpn. 27 (1994) 296-301.

[8] A. Lyngfelt, B. Leckner, T. Mattisson, A fluidized-bed combustion process with inherent CO_2 separation; application of chemical-looping combustion, Chem. Eng. Sci. 56 (2001) 3101-3013.

[9] J. Adánez, A. Abad, F. García–Labiano, P. Gayán, L.F. de Diego, Progress in Chemical Looping Combustion and Reforming Technologies, Progress in Energy and Combustion Science 38 (2012) 215-282.

[10] J. Adánez, L.F. de Diego, F. García-Labiano, P. Gayán, A. Abad, J.M. Palacios,

Selection of oxygen carriers for chemical-looping combustion, Energy & Fuels 18 (2004) 371-377.

[11] T. Mattisson, M. Johansson, A. Lyngfelt, Multicycle reduction and oxidation of different types of iron oxide particles - Application to chemical-looping combustion, Energy & Fuels 18 (2004) 628-637.

[12] M. Johansson, T. Mattisson, A. Lyngfelt, Investigation of Fe_2O_3 with $MgAl_2O_4$ for chemical-looping combustion, Industrial & Engineering Chemistry Research 43 (2004) 6978-6987.

[13] F. García-Labiano, J. Adánez, L.F. de Diego, P. Gayán, A. Abad, Effect of pressure on the behaviour of copper-, iron-, and nickel-based oxygen carriers for chemical looping combustion, Energy Fuels 20 (2006) 26-33.

[14] A. Abad, F. García-Labiano, L.F. de Diego, P. Gayán, J. Adánez, Reduction kinetics of Cu-, Ni- and Fe-based oxygen carriers using syngas ($CO+H_2$) for chemical looping combustion, Energy & Fuels 21 (2007) 1843-1853.

[15] M. Ortiz, L.F. de Diego, P. Gayán, M.A. Pans, F. García-Labiano, A. Abad, J. Adánez, Hydrogen production coupled with CO_2 capture by chemical-looping using mixed Fe-Ni oxygen carriers, Proc 1st Int Conf on Chemical Looping, Lyon, France, 2010.

[16] P. Gayán, M.A. Pans, M. Ortiz, A. Abad, L.F. de Diego, F. García-Labiano, J. Adánez, Testing of a highly reactive impregnated Fe_2O_3/Al_2O_3 oxygen carrier for a SR-CLC system in a continuous CLC unit, Fuel Processing Technology 96 (2012) 37–47.

[17] A. Cabello, C. Dueso, F. García-Labiano, P. Gayán, A. Abad, L.F. de Diego, J. Adánez, Performance of a highly reactive impregnated Fe_2O_3/Al_2O_3 oxygen carrier with CH_4 and H_2S in a 500 W_{th} CLC unit, Fuel 121 (2014) 117-125.

[18] P. Cho, T. Mattisson, A. Lyngfelt, Carbon formation on nickel and iron oxide-containing oxygen carriers for chemical-looping combustion, Industrial & Engineering Chemistry Research 44 (2005) 668-676.

[19] L.F. de Diego, F. García-Labiano, J. Adánez, P. Gayán, A. Abad, A. Cabello, G. Sprachmann, Performance of Cu- and Fe-based oxygen carriers in a 500 W_{th} CLC unit for sour gas combustion with high H_2S content, Submitted for publication.

[20] F. García-Labiano, J. Adánez, L.F. de Diego, P. Gayán, A. Abad, A. Cabello, G. Sprachmann, Energy exploitation of acid gas with high H_2S content by means of a chemical looping combustion system, Submitted for publication.

[21] S.R. Son, S.D. Kim, Chemical-looping combustion with NiO and Fe_2O_3 in a thermobalance and circulating fluidized bed reactor with double loops, Ind. Eng. Chem. Res. 45 (2006) 2689-2696.

[22] A. Abad, T. Mattisson, A. Lyngfelt, M. Johansson, The use of iron oxide as oxygen carrier in a chemical-looping reactor, Fuel 86 (2007) 1021-1035.

[23] A. Lyngfelt, H. Thunman, Construction and 100 h of operational experience of a 10-kW chemical-looping combustor, in: D.C. Thomas, S.M. Benson (Eds.), Carbon dioxide capture for storage in deep geologic formations - Results from the CO_2 capture project, Elsevier, Oxford, UK, 2005, vol. 1, chapter 36.

[24] T. Pröll, K. Mayer, J. Bolhàr-Nordenkampf, P. Kolbitsch, T. Mattisson, A. Lyngfelt, H. Hofbauer, Natural minerals as oxygen carriers for chemical looping combustion in a dual circulating fluidized bed system, Energy Procedia 1 (2009) 27-34.

[25] P. Kolbitsch, J. Bolhàr-Nordenkampf, T. Pröll, H. Hofbauer, Operating experience with chemical looping combustion in a 120 kW dual circulating fluidized bed (DCFB) unit, International Journal of Greenhouse Gas Control 4 (2010) 180-185.

[26] M. Rydén, M. Johansson, E. Cleverstam, A. Lyngfelt, T. Mattisson, Ilmenite with addition of NiO as oxygen carrier for chemical-looping combustion, Fuel 89 (2010) 3523-3533.

[27] P. Moldenhauer, M. Rydén, A. Lyngfelt, Testing of minerals and industrial by-products as oxygen carriers for chemical-looping combustion in a circulating fluidized-bed 300W laboratory reactor, Fuel 93 (2012) 351-363.

[28] M. Ortiz, P. Gayán, L.F. de Diego, F. García-Labiano, A. Abad, M.A. Pans, J. Adánez, Hydrogen production with CO_2 capture by coupling steam reforming of methane and chemical-looping combustion: Use of an iron-based waste product as oxygen carrier burning a PSA tail gas, Journal of Power Sources 196 (2011) 4370-4381.

[29] A. Abad, J. Adánez, F. García-Labiano, L.F. de Diego, P. Gayán, J. Celaya, Mapping of the range of operational conditions for Cu-, Fe-, and Ni-based oxygen carriers in chemical-looping combustion, Chem. Eng. Sci. 62 (2007) 533-549.

[30] K.S. Go, S.R. Son, S.D. Kim, Reaction kinetics of reduction and oxidation of metal oxides for hydrogen production, In J Hydrogen Energy 33 (2008) 5986-5995.

[31] C.D. Bohn, J.P. Cleeton, C.M. Müller, J.F. Davidson, A.N. Hayhurst, S.A. Scott, J.S. Dennis, The kinetics of the reduction of iron oxide by carbon monoxide mixed with carbon dioxide, AIChE Journal 56 (2010) 1016-1029.

[32] J. Bao, Z. Li, H. Sun, N. Cai, Experiment and rate equation modeling of Fe oxidation kinetics in chemical looping combustion, Combustion and Flame 160 (2013) 808–817.

[33] E.R. Monazam, R.W. Breault, R. Siriwardane, G. Richards, S. Carpenter, Kinetics of the reduction of hematite (Fe_2O_3) by methane (CH_4) during chemical looping combustion: A global mechanism, Chemical Engineering Journal 232 (2013) 478–487.

[34] B. Moghtaderi, H. Song, Reduction properties of physically mixed metallic oxide oxygen carriers in chemical looping combustion, Energ. Fuel. 24 (2010) 5359-5368.

[35] E.R. Monazam, R.W. Breault, R. Siriwardane, D.D. Miller, Thermogravimetric Analysis of Modified Hematite by Methane (CH_4) for Chemical-Looping Combustion: A Global Kinetics Mechanism, Ind. Eng. Chem. Res. 52 (2013) 14808-14816.

[36] E. Ksepko, M. Sciazko, P. Babinski, Studies on the redox reaction kinetics of Fe_2O_3–CuO/Al_2O_3 and Fe_2O_3/TiO_2 oxygen carriers, Applied Energy 115 (2014) 374-383.

[37] A. Abad, J. Adánez, A. Cuadrat, F. García-Labiano, P. Gayán, L.F. de Diego, Reaction kinetics of ilmenite for Chemical-Looping Combustion, Chem. Eng. Sci. 66 (2011) 689-702.

[38] S. Nasr, K.P. Plucknet, Kinetics of Iron Ore Reduction by Methane for Chemical Looping Combustion, Energy & Fuels doi: 10.1021/ef402142q.

[39] C. Dong, S. Sheng, W. Qin, Q. Lu, Y. Zhao, X. Wang, J. Zhang, Density functional theory study on activity of α-Fe_2O_3 in chemical-looping combustion system, Applied Surface Science 257 (2011) 8647-8652.

[40] F. Li, Z. Sun, S. Luo, L.S. Fan, Ionic diffusion in the oxidation of iron-effect of support and its implications to chemical looping applications, Energy Environ. Sci. 4 (2011) 876-880.

[41] F. Li, S. Luo, Z. Sun, X. Bao, L.S. Fan, Role of metal oxide support in redox reactions of iron oxide for chemical looping applications: experiments and density functional theory calculations, Energy Environ. Sci. 4 (2011) 3661-3667.

[42] C. Dong, X. Liu, W. Qin, Q. Lu, X. Wang, S. Shi, Y. Yang, Deep reduction behavior of iron oxide and its effect on direct CO oxidation, Applied Surface Science

258 (2012) 2562-2569.

[43] Q. Tan, W. Qin, Q. Chen, C. Dong, W. Li, Y. Yang, Synergetic effect of ZrO_2 on the oxidation–reduction reaction of Fe_2O_3 during chemical looping combustion, Applied Surface Science 258 (2012) 10022-10027.

[44] W. Li, Q. Chen, T. Mi, Density Functional Theory Study of interaction between CO and Oxygen Carrier Fe_2O_3@SBA-15, Advanced Materials Research 610 (2013) 498-501.

[45] D.D. Miller, R. Siriwardane, Mechanism of Methane Chemical Looping Combustion with Hematite Promoted with CeO_2, Energy Fuels 27 (2013) 4087-4096.

[46] W. Qin, Q. Chen, Y. Wang, C. Dong, J. Zhang, W. Li, Y. Yang, Theoretical study of oxidation–reduction reaction of Fe_2O_3 supported on MgO during chemical looping combustion, Applied Surface Science 266 (2013) 350-354.

[47] W. Qin, Y. Wang, C. Dong, J. Zhang, Q. Chen, Y. Yang, The synergetic effect of metal oxide support on Fe_2O_3 for chemical looping combustion: A theoretical study, Applied Surface Science 282 (2013) 718-723.

[48] L. Wang, Q. Li, W. Qin, Z. Zheng, X. Xiao, C. Dong, Activity of Fe_2O_3 and its effect on CO oxidation in the chemical looping combustion: A theoretical account, Advanced Materials Research 726 (2013) 2040-2044.

[49] F. García-Labiano, L.F. de Diego, J. Adánez, A. Abad, P. Gayán, Temperature variations in the oxygen carrier particles during their reduction and oxidation in a Chemical Looping Combustion system, Chem. Eng. Sci. 60 (2005) 851-862.

[50] HSC Chemistry 6.1, Chemical Reaction and Equilibrium Software with Thermochemical Database and Simulation Module, Oututec Research Oy., Pori, Finland. 2008.

[51] Q. Zafar, A. Abad, T. Mattisson, B. Gevert, Reaction Kinetics of a Freeze-Granulated NiO/$MgAl_2O_4$ Oxygen Carrier Particles for Chemical-Looping Combustion, Energy & Fuels 21 (2007) 610-618.

[52] F. García-Labiano, L.F. de Diego, J. Adánez, A. Abad, P. Gayán, Reduction and Oxidation Kinetics of a Copper-Based Oxygen Carrier Prepared by Impregnation for Chemical-Looping Combustion, Ind. Eng. Chem. Res. 43 (2004) 8168-8177.

[53] J.E. Readman, A. Olafsen, J.B. Smith, R. Blom, Chemical Looping Combustion Using NiO/$NiAl_2O_4$: Mechanisms and Kinetics of Reduction-Oxidation (Red-Ox) Reactions from In Situ Powder X-ray Diffraction and Thermogravimetry Experiments, Energy & Fuels 20 (2006) 1382-1387.

[54] C. Dueso, M. Ortiz, A. Abad, F. García-Labiano, L.F. de Diego, P Gayán, J Adánez, Reduction and oxidation kinetics of nickel-based oxygen-carriers for chemical-looping combustion and chemical-looping reforming, Chemical Engineering Journal 188 (2012) 142-154.

[55] O. Levenspiel, Chemical Reaction Engineering, John Wiley and Sons, New York, 1981.

[56] L.F. de Diego, A. Abad, A. Cabello, P. Gayán, F. García-Labiano, J. Adánez, Reduction and Oxidation Kinetics of a $CaMn_{0.9}Mg_{0.1}O_{3-\delta}$ Oxygen Carrier for Chemical-Looping Combustion, Ind. Eng. Chem. Res. 53 (2014) 87-103.

[57] J. Adánez, F. García-Labiano, A. Abad, L.F. de Diego, P. Gayán, Regeneration of Sulfided Dolomite with Steam and Carbon Dioxide, Energy & Fuels 15 (2001) 85-94.

[58] A. Abad, J. Adánez, F. García-Labiano, L.F. de Diego, P. Gayán, Modelling of the chemical-looping combustion of methane using a Cu-based oxygen-carrier, Combustion and Flame 3 (2010) 602-615.

Figure Captions

Fig. 1. TPR profile of fresh particles of the Fe20γAl oxygen carrier.

Fig. 2. Conversion vs time curves during reduction period with CH_4, CO and H_2. Testing conditions: T = 1223 K; reducing gas mixtures: 15 vol% H_2 + 20 vol% H_2O; 15 vol% CO + 20 vol% CO_2; and 15 vol% CH_4 + 20 vol% H_2O (N_2 to balance).

Fig. 3. Effect of H_2O and CO_2 presence on the reduction conversion of the Fe20γAl oxygen carrier with H_2 (a) and CO (b). Testing conditions: T = 1223 K; reducing gases: 5 vol% H_2 and 5 vol% CO.

Fig. 4. Effect of fuel gas concentration on the reduction reaction for CH_4 (a), H_2 (b) and CO (c). T = 1223 K. The continuous lines are results predicted by the model using kinetic parameters obtained in this work.

Fig. 5. Effect of the temperature on the reduction reaction of the Fe20γAl oxygen carrier. Reducing gas mixtures: (a) 15 vol% CH_4 + 20 vol% H_2O; (b) 15 vol% CO + 20 vol% CO_2; (c) 15 vol% H_2 + 20 vol% H_2O; and (d) 5 vol% H_2 + 48 vol.% H_2O. The continuous lines are results predicted by the model using kinetic parameters obtained in this work.

Fig. 6. Effect of O_2 concentration on the oxidation reaction of the Fe20γAl oxygen carrier. Operating conditions: T = 1223 K. The continuous lines are results predicted by the model using kinetic parameters obtained in this work.

Fig. 7. Effect of temperature on the oxidation reaction of the Fe20γAl oxygen carrier with O_2 (10 vol%). The continuous lines are results predicted by the model using kinetic parameters obtained in this work.

Fig. 8. Scheme of the reacting mechanism for CH_4 reduction with the Fe20γAl oxygen carrier.

Fig. 9. Plot of ln (C_i) vs. ln ($1/\tau_{ch}$) to obtain the reaction order with respect to CH_4, H_2, CO and O_2.

Fig. 10. Arrhenius plots to determine activation energy for k_s (a), and effective product layer diffusivity, D_{pl} (b), for the reaction of CH_4, H_2, CO and O_2 with the Fe20γAl oxygen carrier.

Fig. 11. Solids circulation rate vs variation of solids conversion in the fuel reactor using the Fe20γAl material as oxygen carrier. Reducing gas: CH_4.

Fig. 12. Variation of reduction conversion in chemically controlled reaction for Fe20γAl material reached in the fuel reactor for CH_4, H_2 and CO combustion in a usual range of operating temperatures for CLC.

Fig. 13. Total solids inventory of the Fe20γAl material as a function of the solids conversion at the inlet of the fuel reactor ($X_{S,ox\ in,FR}$). Reducing agent: CH_4. $\Delta X_S = 0.25$. T = 1223 K. It is assumed that the Fe20γAl oxygen carrier is only reduced up to solids conversion values within the range at which the reaction kinetics is controlled by chemical reaction.

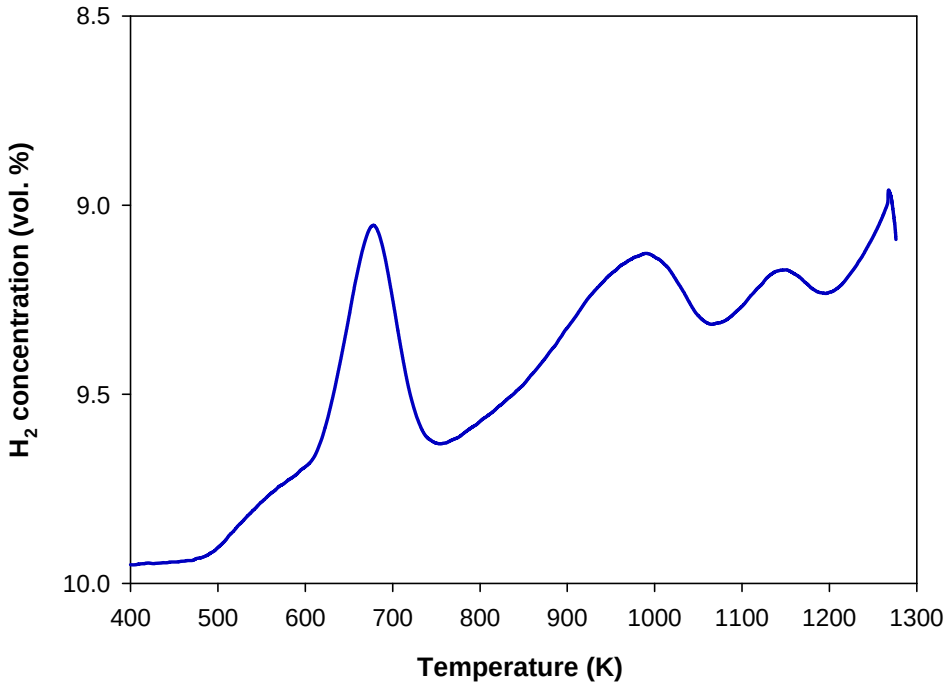

Fig. 1. TPR profile of fresh particles of the Fe20γAl oxygen carrier.

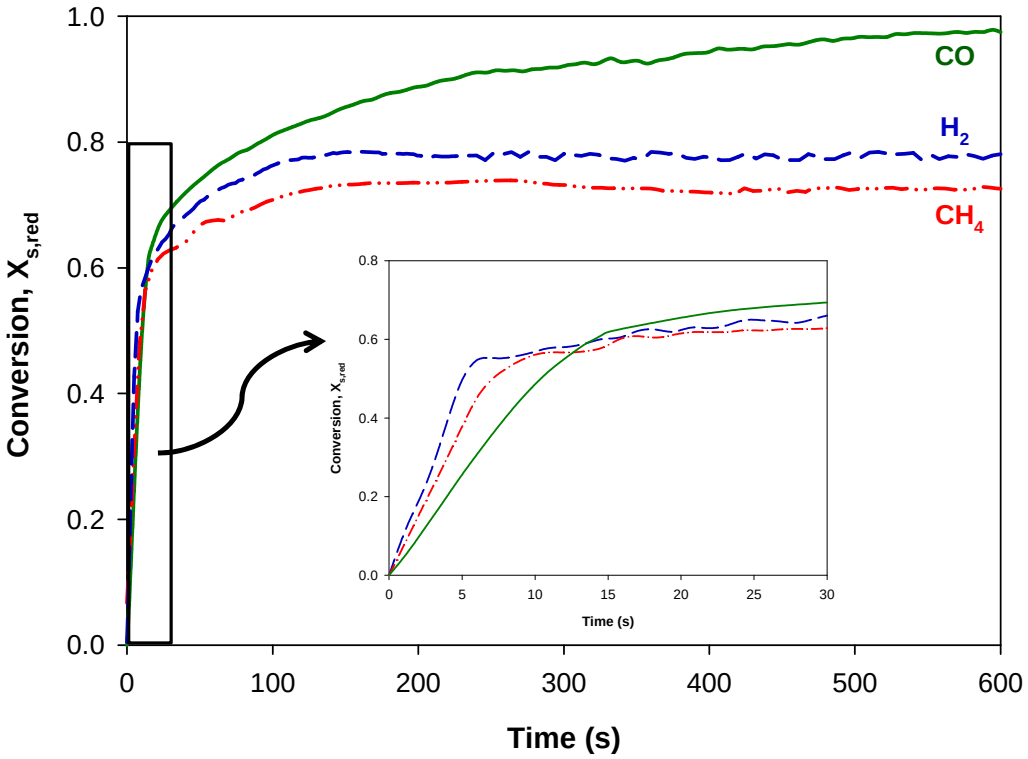

Fig. 2. Conversion vs time curves during reduction period with CH_4, CO and H_2. Testing conditions: T = 1223 K; reducing gas mixtures: 15 vol% H_2 + 20 vol% H_2O; 15 vol% CO + 20 vol% CO_2; and 15 vol% CH_4 + 20 vol% H_2O (N_2 to balance).

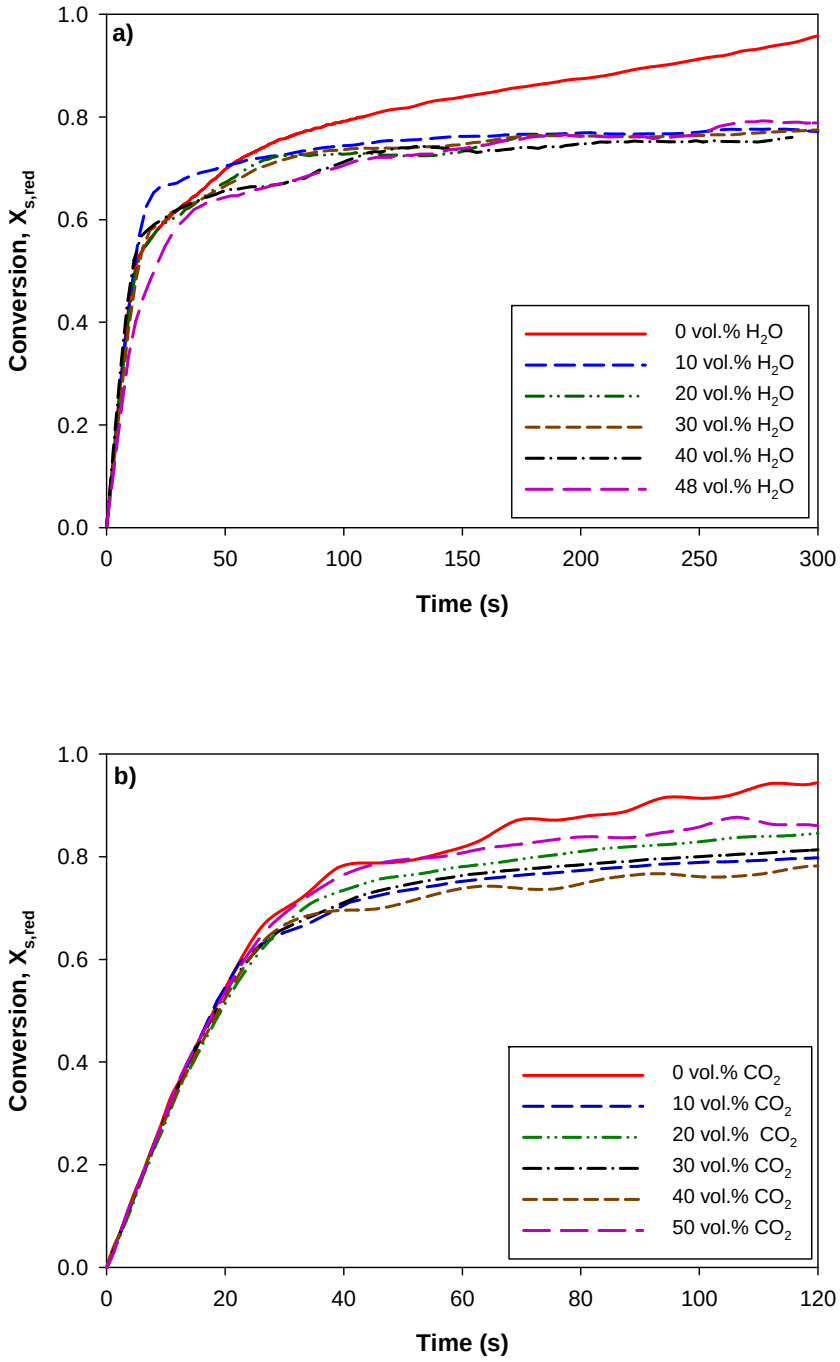

Fig. 3. Effect of H_2O and CO_2 presence on the reduction conversion of the Fe20γAl oxygen carrier with H_2 (a) and CO (b). Testing conditions: T = 1223 K; reducing gases: 5 vol% H_2 and 5 vol% CO.

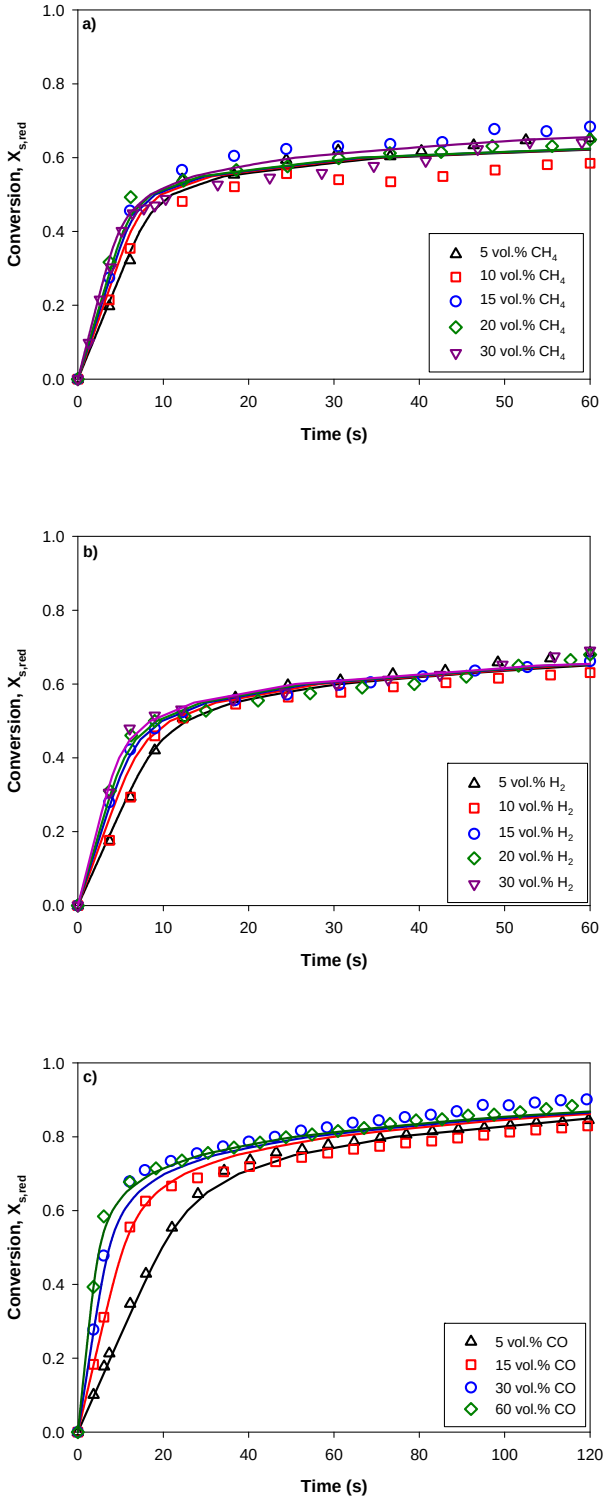

Fig. 4. Effect of fuel gas concentration on the reduction reaction for CH_4 (a), H_2 (b) and CO (c). T = 1223 K. The continuous lines are results predicted by the model using kinetic parameters obtained in this work.

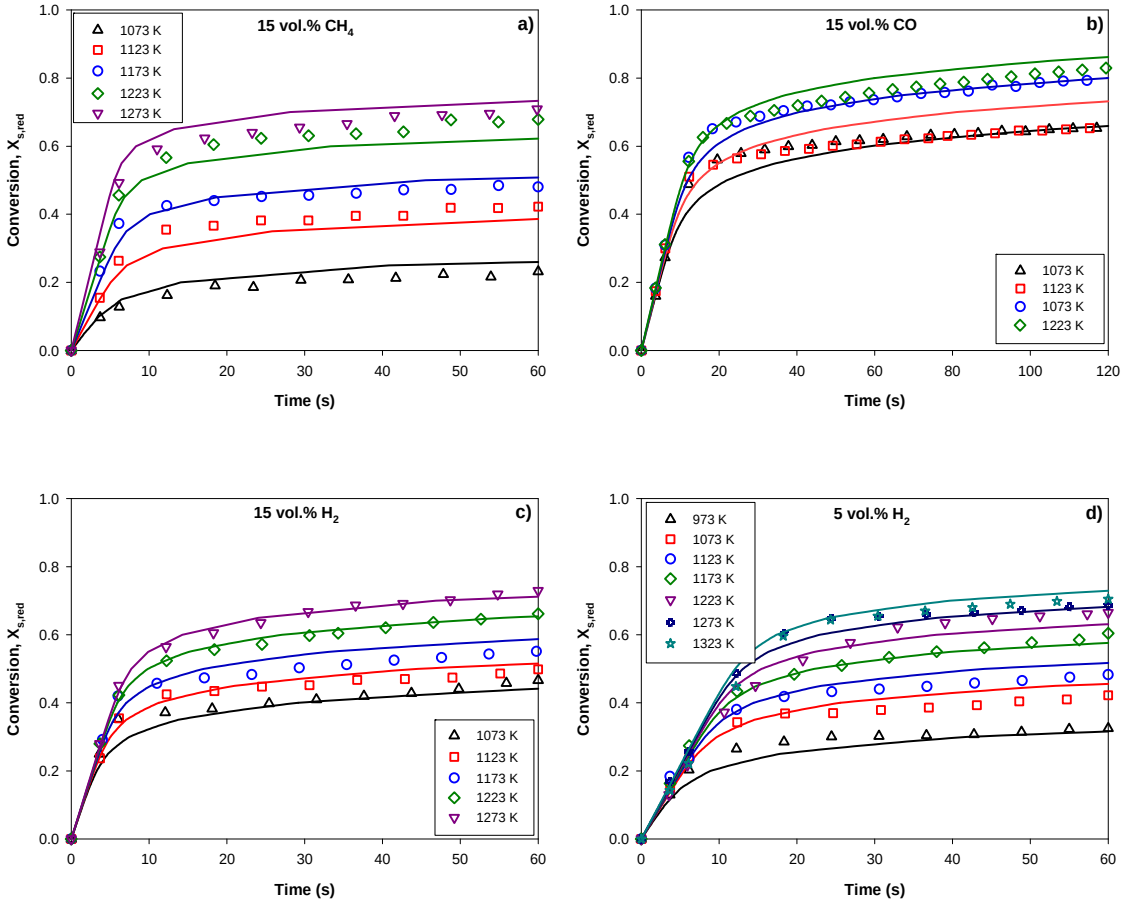

Fig. 5. Effect of the temperature on the reduction reaction of the Fe20γAl oxygen carrier. Reducing gas mixtures: (a) 15 vol% CH_4 + 20 vol% H_2O; (b) 15 vol% CO + 20 vol% CO_2; (c) 15 vol% H_2 + 20 vol% H_2O; and (d) 5 vol% H_2 + 48 vol% H_2O. The continuous lines are results predicted by the model using kinetic parameters obtained in this work.

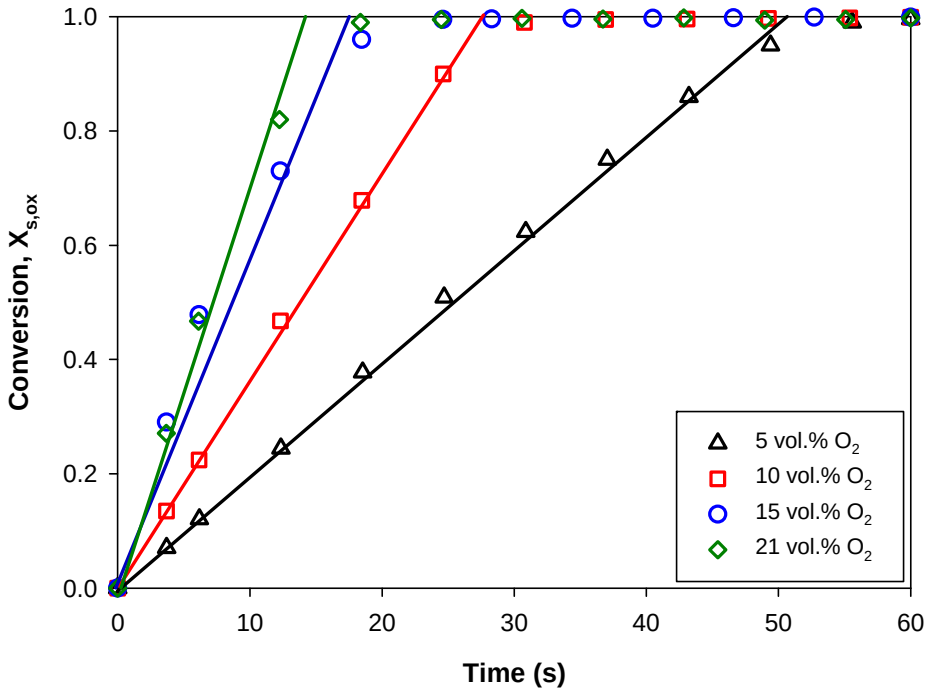

Fig. 6. Effect of O_2 concentration on the oxidation reaction of the Fe20γAl oxygen carrier. Operating conditions: T = 1223 K. The continuous lines are results predicted by the model using kinetic parameters obtained in this work.

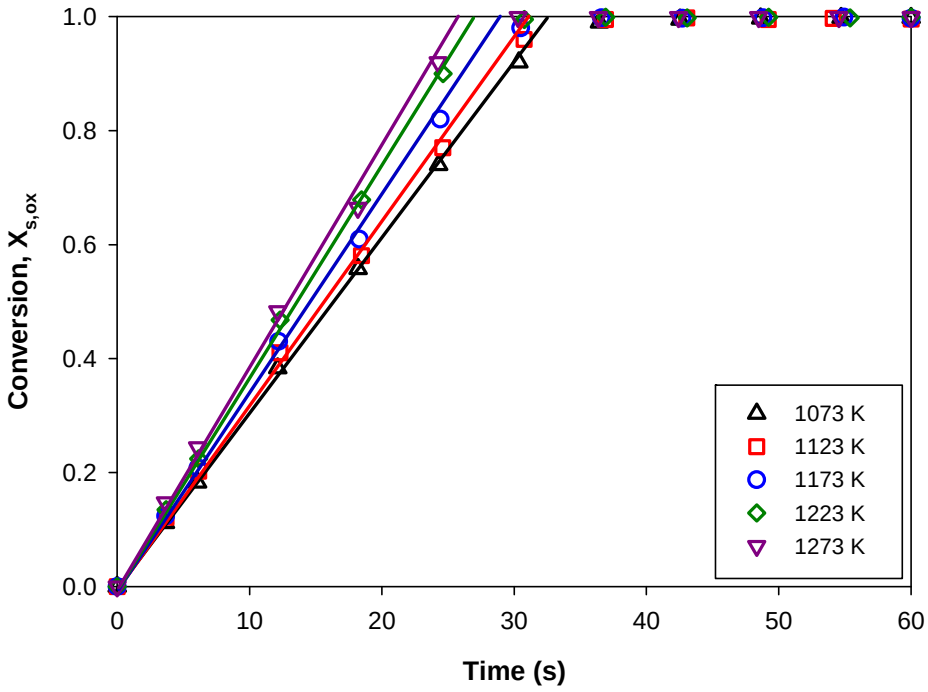

Fig. 7. Effect of temperature on the oxidation reaction of the Fe20γAl oxygen carrier with O_2 (10 vol%). The continuous lines are results predicted by the model using kinetic parameters obtained in this work.

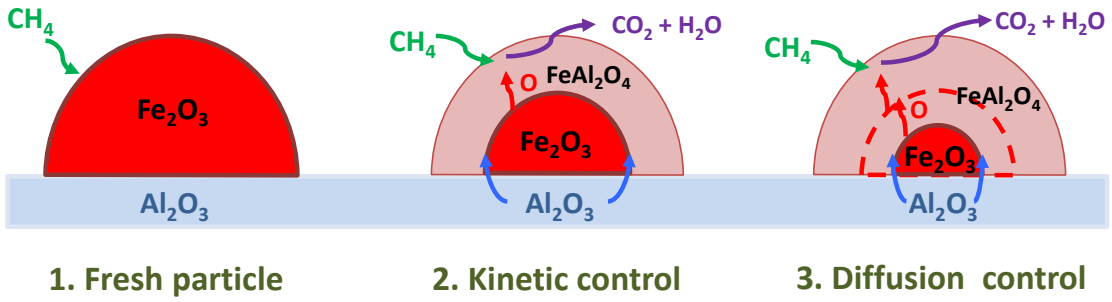

Fig. 8. Scheme of the reacting mechanism for CH_4 reduction with the Fe20γAl oxygen carrier.

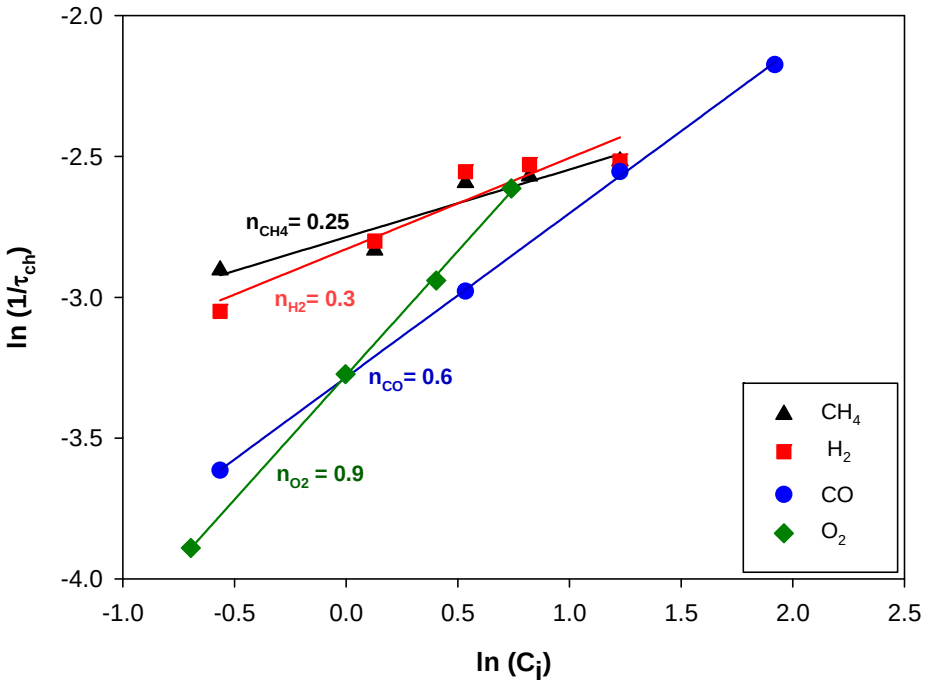

Fig. 9. Plot of ln (C_i) vs. ln ($1/\tau_{ch}$) to obtain the reaction order with respect to CH_4, H_2, CO and O_2.

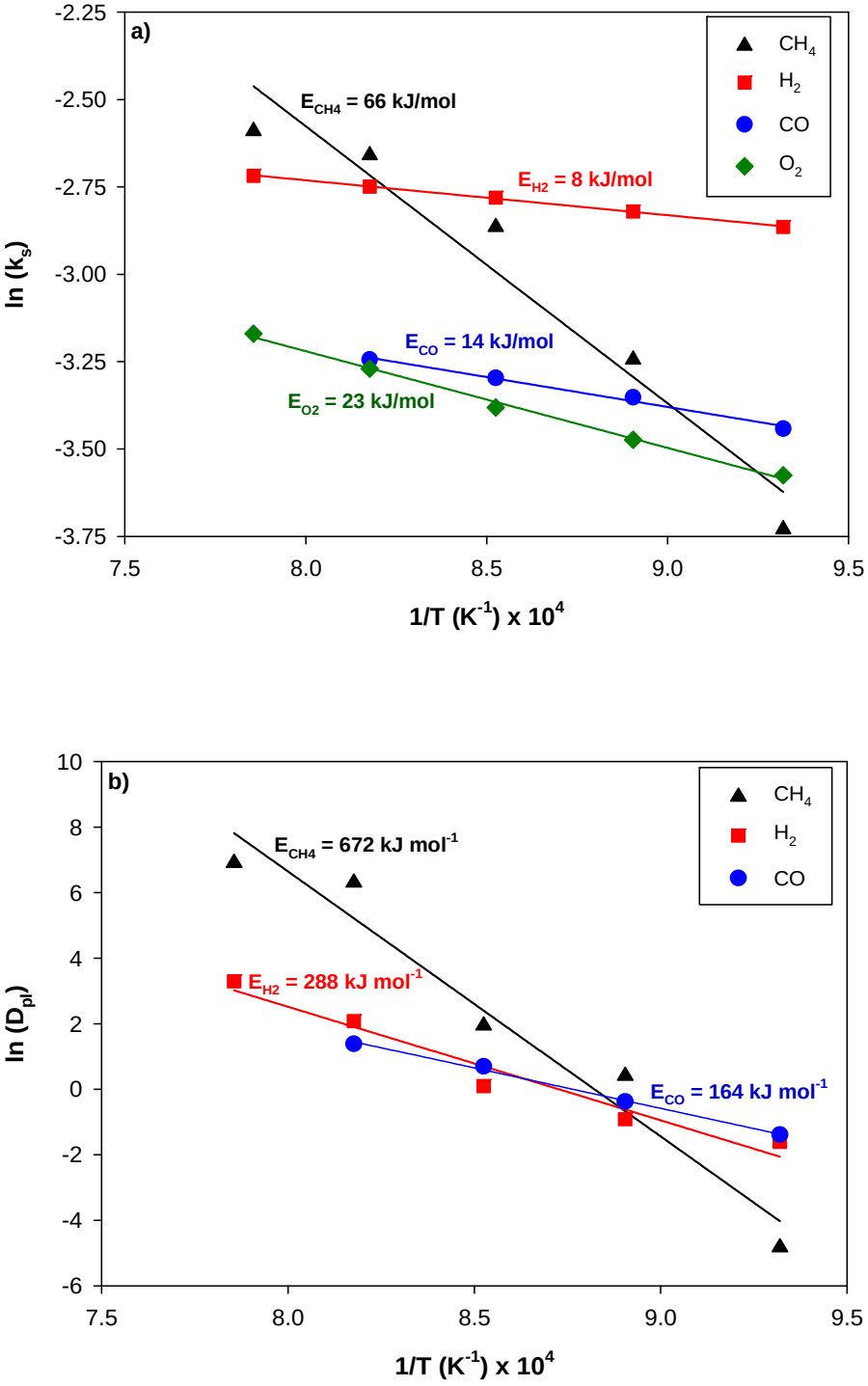

Fig. 10. Arrhenius plots to determine the activation energy for k_s (a), and the effective product layer diffusivity, D_{pl} (b), for the reaction of CH_4, H_2, CO and O_2 with the Fe20γAl oxygen carrier.

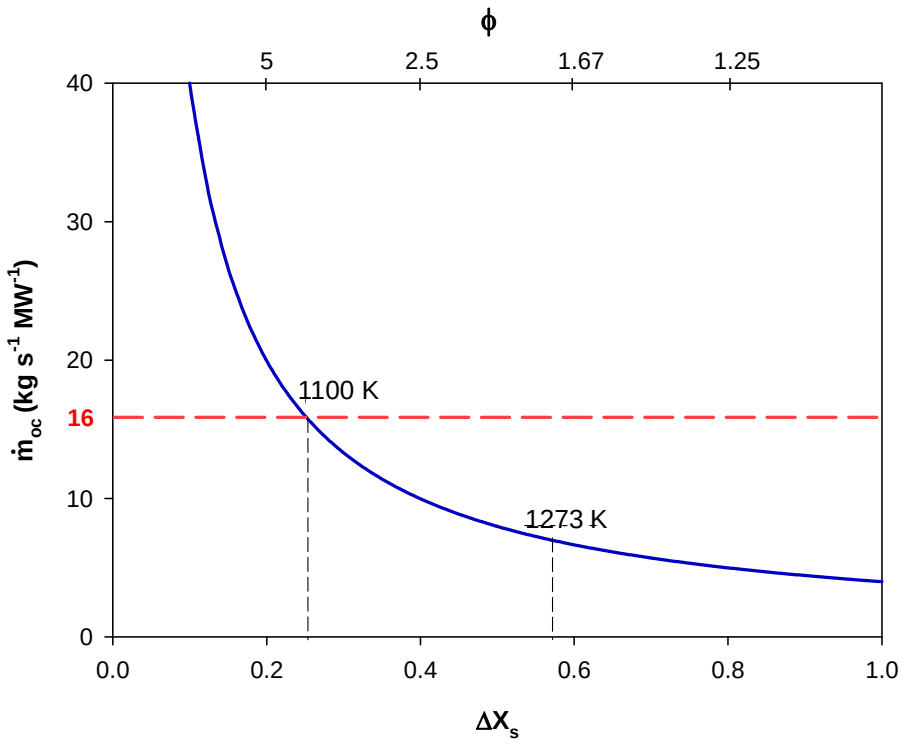

Fig. 11. Solids circulation rate vs the variation of solids conversion in the fuel reactor using Fe20γAl material as oxygen carrier. Reducing gas: CH_4.

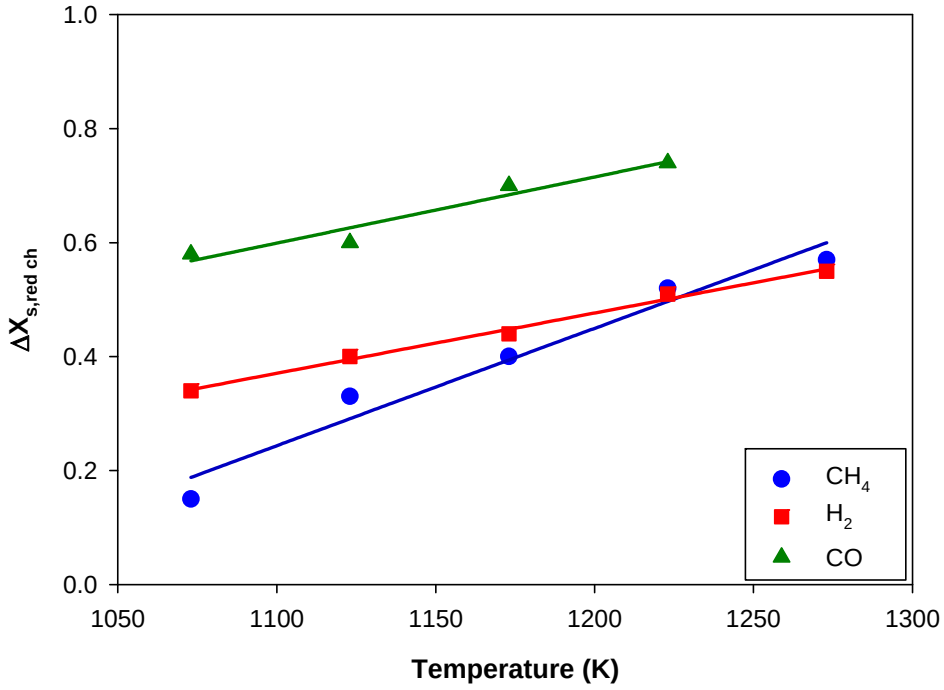

Fig. 12. Variation of reduction conversion in chemically controlled reaction for Fe20γAl material reached in the fuel reactor for CH_4, H_2 and CO combustion in a usual range of operating temperatures for CLC.

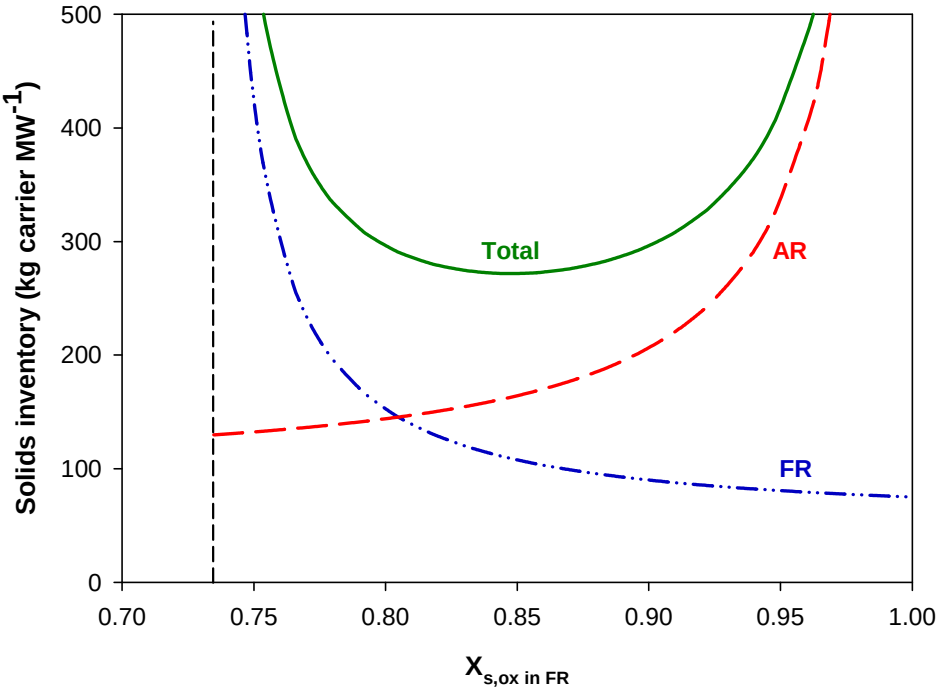

Fig. 13. Total solids inventory of the Fe20γAl material as a function of the solids conversion at the inlet of the fuel reactor ($X_{S,ox\ in,FR}$). Reducing agent: CH_4. $\Delta X_S = 0.25$. T = 1223 K. It is assumed that the Fe20γAl oxygen carrier is only reduced up to solids conversion values within the range at which the reaction kinetics is controlled by chemical reaction.

Tables

Table 1. Summary of kinetic data for Fe-based oxygen carriers.

Oxygen carrier	Method of preparation	Experimental conditions	Kinetic Model	Redox system	Reference
Fe_2O_3 d_p = 125µm Roc= 10.0%	Solid state calcination	TGA; T = 773-1173 K CH_4	Diffusion control n = n.a.; E_{act} = 271kJ/mol	Fe_2O_3/ FeO	[30]
Fe_2O_3 d_p = 300-425µm R_{OC} = 3.3-10.0%	Mechanical mixing	Fluid bed; T = 723-1123 K 1.5-10 vol.% CO	DRM n = 1.0; E_{act} = 75 kJ/mol n = 1.0; E_{act} = 94 kJ/mol	 Fe_2O_3/Fe_3O_4 Fe_3O_4/FeO	[31]
Multi-crystal Fe d_p = n.a. R_{OC} = 30.0%	n.a.	TGA; T = 973-1173 K 0.07-5.25 vol.% O_2	Nucleation and growth model n = n.a.; E_{act} = n.a.	Fe_2O_3/Fe	[32]
94 wt.% Fe_2O_3 d_p = 60-100µm Roc = 9.4%	Crush and sieve	TGA; T = 973-1098 K 15-35 vol.% CH_4	Two parallel reactions (R1 and R2) R1: n = n.a.; E_{act} = 34kJ/mol R2: nucleation and grow model; n = n.a.; E_{act} = 39kJ/mol	 Fe_3O_4/FeO Fe_2O_3/Fe_3O_4	[33]
45 wt.% Fe_2O_3 on Al_2O_3 d_p = 90-250µm R_{OC} = 1.3%	Impregnation	TGA; T = 773-1273 K Total pressure: 1-30 atm 5-70 vol.% H_2 5-70 vol.% CO 5-21 vol.% O_2	CGSM n = 0.8; E_{act} = 24 kJ/mol n = 1.0; E_{act} = 20 kJ/mol n = 1.0; E_{act} = 14 kJ/mol	Fe_2O_3/Fe_3O_4	[13]
58 wt.% Fe_2O_3 on Al_2O_3 d_p = 90-106µm R_{OC} = 4.0%	Mechanical mixing	TGA; T = 1073-1123 K 20-70 vol.% CH_4 20-70 vol.% H_2 20-70 vol.% CO	SCM with Fg=3 n = 0.2; E_{act} = 45 kJ/mol n = 0.85; E_{act} = 22 kJ/mol n = 1.0; E_{act} = 19 kJ/mol	Fe_2O_3/Fe_3O_4-$FeAl_2O_4$	[34]
60 wt.% Fe_2O_3 on Al_2O_3 d_p = 90-250µm R_{OC} = 4.1%	Freeze granulation	TGA; T = 873-1223 K 5-70 vol.% CH_4 5-70 vol.% H_2 5-70 vol.% CO 5-21 vol.% O_2	SCM with Fg=3 n = 1.3; E_{act} = 49 kJ/mol n = 0.5; E_{act} = 24 kJ/mol n = 1.0; E_{act} = 20 kJ/mol n = 1.0; E_{act} = 14 kJ/mol	Fe_2O_3/Fe_3O_4-$FeAl_2O_4$	[14,29]
60 wt.% Fe_2O_3 on bentonite d_p = 106-150µm R_{OC} = 2.0%	Mechanical mixing	TGA; T = 973-1273 K 10 vol.% CH_4 10 vol.% O_2	Red: MVM; Ox: SCM n = n.a.; E_{act} = 29 kJ/mol n = n.a.; E_{act} = 6 kJ/mol	Fe_2O_3/Fe_3O_4	[21]
75-95 wt.% Fe_2O_3 on MgO d_p = 100-300µm R_{OC} = 7.5-9.5%	Hot incipient wetness impregnation	TGA; T = 973-1098 K 5-20 vol.% CH_4	Two-competing reactions (R1 and R2) R1: n = n.a; E_{act} = 50kJ/mol R2: n = n.a; E_{act} = 65kJ/mol	 Fe_2O_3/Fe_3O_4 Fe_3O_4/FeO	[35]
80 wt.% Fe_2O_3 on TiO_2 d_p < 250µm Roc= 2.7-24.0%	Solid-state mixing	TGA; T = 873-1223 K 3 vol.% H_2 in Ar Air	Red:VM; Ox: SCM n= n.a.; E_{act} = 34 kJ/mol n= n.a.; E_{act}= 0 kJ/mol	Fe_2O_3/Fe_3O_4-FeO-Fe	[36]
Pre-oxidized ilmenite (Fe_2TiO_5) d_p = 150-300µm R_{OC} = 4.0%	Thermal treatment	TGA; T = 1073-1123 K 5-50 vol.% CH_4 5-50 vol.% H_2 5-50 vol.% CO 5-21 vol.% O_2	SCM with Fg=3 n = 1.0; E_{act} = 165 kJ/mol n = 1.0; E_{act} = 109 kJ/mol n = 1.0; E_{act} = 113 kJ/mol n = 1.0; E_{act} = 12 kJ/mol	$Fe_2O_3 \cdot TiO_2$/ $FeO \cdot TiO_2$	[37]
Activated ilmenite (Fe_2TiO_5) d_p = 150-300µm R_{OC} = 3.3%	Thermal treatment + activation in a fluidized bed	TGA; T = 1073-1123 K 5-50 vol.% CH_4 5-50 vol.% H_2 5-50 vol.% CO 5-21 vol.% O_2	SCM with Fg=3 n = 1.0; E_{act} = 136 kJ/mol n = 1.0; E_{act} = 65 kJ/mol n = 0.8; E_{act} = 80 kJ/mol n = 1.0; E_{act} = 25 kJ/mol	$Fe_2O_3 \cdot TiO_2$/ $FeO \cdot TiO_2$	[37]
98 wt.% Fe_2O_3 d_p = 50-200µm Roc = 3.2%	Crush and sieve	TGA; T = 1073-1223 K 33 vol.% CH_4	Avrami-Erofe'ev phase change model n= n.a.; E_{act} = 215 kJ/mol	Fe_2O_3/Fe_3O_4	[38]

Table 2. Main physicochemical properties of the Fe20γAl material

	Fresh material
Fe_2O_3 (wt. %)	20[1]
Oxygen transport capacity, R_{OC}	0.02
Particle size (μm)	200-400
Skeletal density (kg m^{-3})	3950
Crushing strength (N)	1.5
Porosity (%)	50.5
Specific surface area, BET (m^2 g^{-1})	39.1
XRD	Fe_2O_3, α-Al_2O_3

[1] Determined by ICP-AES.

Table 3. Kinetic parameters for reaction of Fe20γAl oxygen carrier particles with reducing (CH_4, H_2, CO) and oxidizing gases (O_2).

		Units	**CH_4**	**H_2**	**CO**	**O_2**
n	Order of the reaction	---	0.25	0.3	0.6	0.9
$k_{s,0}$	Pre-exponential factor of k_s	$m^{3n}\ mol^{-n}\ s^{-1}$	$4.34 \cdot 10^{1}$	$1.45 \cdot 10^{-1}$	$1.59 \cdot 10^{-1}$	$3.64 \cdot 10^{-1}$
E_{ch}	Activation energy for k_s	kJ/mol	66	8	14	23
n’	Order of diffusion	---	0	0	0	---
$D_{pl,0}$	Pre-exponential factor of D_{pl}	$m^{3n'}\ mol^{-n'}\ s^{-1}$	$9.80 \cdot 10^{30}$	$1.40 \cdot 10^{13}$	$2.29 \cdot 10^{9}$	---
E_{pl}	Activation energy for D_{pl}	kJ/mol	672	288	204	---
$k_{X,0}$	Pre-exponential factor of k_X	---	20	14	10	---
E_X	Activation energy for k_X	kJ/mol	0	0	0	---

Table 4. Minimum solids inventories for CH_4, H_2 and CO combustion in fuel and air reactors of a CLC unit with Fe20γAl as oxygen carrier (T = 1223 K).

	CH_4	**H_2**	**CO**
Min. solids inventory in FR (kg)	54	37	42
Min. solids inventory in AR (kg)	95	79	68
Min. total solids inventory (kg)	149	116	109

Appendix A. Determination of solids inventory. Modification to the calculation method proposed by Abad et al. [29] considering that complete reduction of the oxygen carrier was not possible owing to diffusional limitations.

Considering the reaction kinetics obtained in this work, it can be assumed that diffusion-controlled reaction does not take place to any relevant extension in a CLC unit because this takes much more time than the average residence time of particles in the fuel reactor. Thus, additional expressions were defined in order to calculate the total solids inventory in the fuel reactor for the case where the oxygen carrier is only reduced up to solids conversion values within the range at which the reduction is controlled by chemical reaction.

Thus, the solids conversion had to be recalculated to be used in Eqs (22) and (23). Namely, the active Fe_2O_3 content, and therefore the actual oxygen transport capacity R'_{OC}, depends on the $X_{S,red\ ch}$ value shown in Fig. 12 as

$$R'_{OC} = X_{S,red\ ch} \cdot R_{OC} \tag{A.1}$$

Therefore, the solid fraction reacting with slow diffusion-controlled reaction is assumed to be inert. The solids inventory in the fuel reactor can be calculated in these conditions as follows:

$$m_{OC,FR} = \frac{2 \cdot d \cdot M_O}{\Delta H_C^0} \cdot \frac{\tau'_r}{R'_{OC}} \cdot \frac{1}{\Phi'_{FR}} \tag{A.2}$$

Fig. A.1 (a) illustrates an example of a conversion vs time curve for CH_4 combustion from which both τ'_r and $X_{S,red\ ch}$ parameters can be calculated. $X_{S,red\ ch}$ is the maximum conversion reached by the oxygen carrier particles when the reduction reaction is controlled by chemical reaction. The time corresponding to this reduction conversion is

defined as $\tau_r^{'}$. The calculation method considers a modified conversion $X_{S,\,red}^{'}$, which ranges from 0 to 1 when the solids conversion varies from 0 to $X_{S,\,red\,ch}$. $\tau_r^{'}$ can be determined at each temperature and reducing gas concentration with the kinetic data obtained in this work as

$$\tau_r^{'} = \Delta X_{s,red\ ch}\tau_r \tag{A.3}$$

Thus, it was deduced that

$$\frac{\tau_r}{R_{OC}} = \frac{\tau_r^{'}}{R_{OC}^{'}} \tag{A.4}$$

and consequently, Eq. (A.2) can be written as

$$m_{OC,FR} = \frac{2 \cdot d \cdot M_O}{\Delta H_C^0} \cdot \frac{\tau_r}{R_{OC}} \cdot \frac{1}{\Phi_{FR}^{'}} \tag{A.5}$$

The characteristic reactivity in the fuel reactor was also redefined according to the following expression:

$$\Phi_{FR}^{'} = 1 - \exp\left(- \frac{\left(1 - X_{S,red\ in\ FR}^{'}\right)}{\Delta X_S^{'}} \Phi_{FR}^{'} \right) \tag{A.6}$$

where $X_{S,red\ in\ FR}^{'}$ and $\Delta X_S^{'}$ are calculated as (see Fig. A1 (b)):

$$X_{S,red\ in\ FR}^{'} = \frac{X_{S,red\ in\ FR}}{X_{S,red\ ch}}, \qquad X_{S,red\ in\ FR} < X_{S,red\ ch} \tag{A.7}$$

$$\Delta X_S^{'} = \frac{\Delta X_S}{X_{S,red\ ch}}, \qquad \Delta X_S < X_{S,red\ ch} \tag{A.8}$$

Furthermore, $X_{s,ox\ in\ FR}^{'}$ can be calculated as:

$$X'_{S,ox\ in\ FR} = \frac{X_{S,ox\ in\ FR} - X_{S,ox\ \min}}{1 - X_{S,ox\ \min}} \tag{A.9}$$

Considering that $X_{S,ox\ \min} = 1 - X_{S,red\ ch}$, $X_{S,ox\ in\ FR}$ can be defined according to Eq. (A.10) as follows:

$$X_{S,ox\ in\ FR} = X'_{S,ox\ in\ FR} \cdot X_{S,red\ ch} + \left(1 - X_{S,red\ ch}\right) \tag{A.10}$$

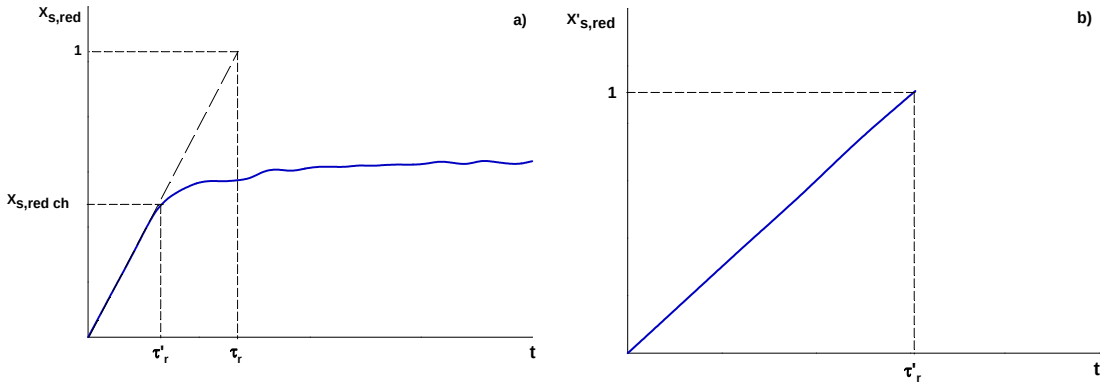

Fig. A.1. (a) Determination of $\tau_r^{'}$ and $X_{S,red\,ch}$ parameters from reduction conversion vs time curve (Fig. 5a). (b) Normalized reduction conversion vs time curve when the reduction reaction is controlled by chemical reaction. Operating conditions: reducing gas, 15 vol% CH_4; temperature: 1223 K.